# NASA TECHNICAL MEMORANDUM

NASA TM-82423

# UNDERCOOLING MEASUREMENT IN A LOW-GRAVITY CONTAINERLESS ENVIRONMENT

By Michael B. Robinson
Space Sciences Laboratory

May 1981

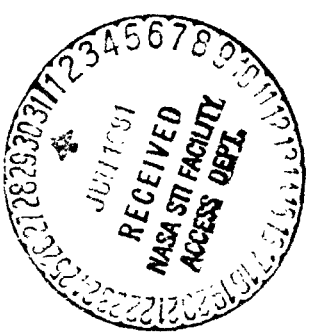


**NASA**

*George C. Marshall Space Flight Center*
*Marshall Space Flight Center, Alabama*

TABLE OF CONTENTS

## LIST OF ILLUSTRATIONS

LIST OF ILLUSTRATIONS (continued)

## LIST OF SYMBOLS

| | |
|---|---|
| $A$ | Surface area of spherical drop |
| $A_n$ | Cross-sectional area of the support wire |
| $C$ | Specific heat |
| $C_2$ | A constant equal to 1.43 cm-K |
| $H_f$ | Heat of fusion |
| $H_v$ | Heat of evaporation |
| $K$ | Thermal conductivity |
| $K_o$ | $\epsilon_T A\sigma/mC$ |
| $m$ | Mass of drop |
| $\Delta m$ | Mass loss during heating, melting, and cooling |
| $\dot{Q}$ | Rate of heat loss |
| $\dot{Q}_{cn}$ | Heat conducted through the $n^{th}$ incremental element of the support wire |
| $\dot{Q}_I$ | Power input to the sample |
| $\dot{Q}_N$ | Radiation power emitted by a drop at the nucleation temperature |
| $\dot{Q}_R$ | Heat loss by radiation |
| $\dot{Q}_{Rn}$ | Heat loss by radiation from the $n^{th}$ incremental element of the support wire |
| $\dot{Q}_w$ | Heat loss due to the support wire |
| $\Delta\dot{Q}$ | Change in the brightness of a drop due to recalescence |
| $R_w$ | Radius of the support wire |
| $S_n$ | Surface area of $n^{th}$ incremental element of the support wire |
| $T$ | Temperature of a drop |
| $T_B$ | Brightness temperature as measured by the automatic optical pyrometer |
| $T_c$ | Superconducting transistor temperature |
| $T_f$ | Final temperature |

## LIST OF SYMBOLS (concluded)

| | |
|---|---|
| $T_i$ | Temperature of a drop at the time of release into the drop tube |
| $T_m$ | Melting temperature |
| $T_n$ | Temperature of the $n^{th}$ incremental element of the support wire |
| $T_N$ | Temperature of a drop at the time of nucleation |
| $T_o$ | Ambient temperature |
| $T_{ov}$ | Amount of overheating above the melting temperature |
| $T_s$ | Temperature of droplet attached to support wire |
| $T_t$ | True temperature of the sample |
| $T_u$ | Amount of undercooling |
| $\Delta T$ | Change in temperature |
| $\Delta T_c$ | Amount of cooling |
| $\Delta T_j$ | Small change in temperature |
| $t_c$ | Cooling time |
| $t_{cj}$ | Time to cool $\Delta T_j$ |
| $t_s$ | Solidification time |
| X | Distance along support wire |

Greek

| | |
|---|---|
| $\alpha$ | Length of each of the n incremental elements of the support wire |
| $\beta$ | A constant which exponentially describes the temperature profile along the support wire |
| $\epsilon_s$ | Spectral emissivity |
| $\epsilon_T$ | Total hemispherical emissivity |
| $\epsilon_w$ | Total hemispherical emissivity of the support wire |
| $\lambda$ | Operating wavelength of the automatic optical pyrometer (0.65 $\mu$m) |
| $\sigma$ | Boltzmann's constant ($5.67 \times 10^{-12}$ W/cm$^2$ - K$^4$) |

# I. INTRODUCTION

Undercooling is achieved when a material is cooled below its equilibrium melting temperature and is maintained in the liquid state. If the material is cooled further, it will undercool further until at some point nucleation will occur and solidification begins. After nucleation, the undercooled liquid will solidify very quickly, giving up the latent heat of fusion associated with this phase change. This sudden release of heat will increase the temperature of the solid material back to or near its melting point. The sudden increase in temperature due to the release of the heat of fusion is defined as recalescence.

An undercooled liquid solidifies when the liquid nucleates and crystal growth begins from some point which first adds crystalline structure to the liquid. This point, or nucleation site, could be such things as crucible walls, impurities, shock waves propagating through the liquid, or pieces of unmolten sample material. A question remains as to what is the maximum amount a material can be undercooled. One theory is that, in the absence of all heterogeneous nucleation sites, an undercooled liquid will reach a maximum undercooling at which point homogeneous nucleation will occur. Turnbull has experimentally determined a proposed homogeneous nucleation limit for various pure metals to be approximately 18 percent of the melting point [1]. Therefore, a material with a melting temperature, $T_m$, of 1000 K would not be expected to undercool more than 0.18 $T_m$ or 180 K, which corresponds to a temperature of 820 K for the undercooled liquid. Another theory is that there is no intrinsic property of materials which will not allow them to undercool past a certain point but that all nucleation is heterogeneously determined. Perepezko and Rasmussen [2] have recently reported undercoolings of up to 0.5 $T_m$ for certain low melting temperature metals and alloys such as Ga.

Undercooling has been shown to significantly affect the solidification process, resulting in changes in solidification speeds [3], microstructures [4, 5, 6], alloy solid solubility [7], and homogeneity [8]. Undercooling also has enhanced the formation of

metastable phases not present on the equilibrium phase diagram [2, 7]. It should, therefore, be possible to form, through undercooling, technologically important metastable phases with unique material properties.

Undercooling has been achieved by many different techniques. One technique involves breaking the sample material into small (5 to 200 $\mu$m) particles. Since there is considered to be a limited number of heterogeneous nucleation sites within the starting sample, only a fraction of the smaller droplets will be expected to contain these nucleation sites. Therefore, most of the particles will be expected to undercool. The particles can either be placed on a heated microscope slide with melting and undercooling being optically observed [1] or emulsified in a carrier fluid which does not act as a nucleating agent. Emulsified droplets have been observed to undercool by dilatometry [9] or more recently by differential thermal analysis, DTA [2]. Also, Walker [4] and others [5, 6] have undercooled bulk samples, instead of small drops, by cooling in amorphous crucibles.

Techniques have also been developed to undercool molten drops of metals and alloys in a containerless environment. One technique involves the use of electromagnetic levitators [10], which provides a containerless but not quiescent environment due to the large convective currents induced in the molten sample. Meyer and Rinderer [11] have produced containerless undercooled droplets by discharging capacitors into sample wires of diameters of 0.1 and 0.5 mm which melt and break into droplets due to the capillary and pinch instabilities of the molten wire. The droplets were cooled in a helium atmosphere with recalescence being photographed to show undercooling. Cech and Turnbull [12] have used short drop tubes to undercool small metal droplets. Nelson [13] used pulsed laser heating and short drop tubes to study undercooling in small drops of refractory metals.

A low-gravity environment has been postulated as conducive to containerless undercooling because it provides a quiescent environment. A containerless low-gravity environment can be achieved for short periods of time by the use of long drop tubes [14]. A long drop tube offers several advantages for the undercooling of samples over previous containerless techniques. High-temperature metals and alloys can be melted and undercooled. Also, samples need not be limited to small ($< 200$ $\mu$m) sizes but instead can be studied in the bulk

(1 to 5 mm diameter). Thus, it should be possible to undercool technologically important high-temperature bulk samples to the maximum extent possible. Niobium drops of 3 to 5 mm diameter have been undercooled to 19 percent of the melting temperature of 2741 K in a 32 m drop tube [14]. Another advantage of long drop tubes is that, due to the increased free-fall time, it is possible to study the low gravity effect on solidification to a much better degree than previous undercooling techniques. Also, long drop tubes have been used to form amorphous drops of $Pd_{77.5}Si_{16.5}Cu_6$ of up to 1.5 mm diameter [15].

While undercooling in a long drop tube offers many advantages, it is also difficult to provide accurate undercooling data for molten drops free-falling over long distances. The purpose of this study was to develop and discuss a technique for measurement of undercooling of molten droplets cooling in a long drop tube. The described technique should also be applicable to measuring undercooling in any low-gravity containerless processing technique. This study is part of a larger group activity to study the undercooling of peritectic superconducting alloys. The group consists of Lewis Lacy; Tom Rathz; and the author; all of Marshall Space Flight Center, Alabama.

The material used for this study was pure (99.99%) niobium and niobium-germanium alloys of 13, 18, and 22 atomic percent (a/o) germanium. The Nb-Ge alloys are technically important since such alloys possess a high superconducting transition temperature ($T_c$) metastable phase of $Nb_3Ge$ of the A-15 structure. This metastable phase, called $\beta$, has previously been formed only in small samples. One formation technique involves the production of the $\beta$ phase in the form of a thin film [16, 17]. Thin film samples have resulted in samples with a $T_c$ as high as 22 K. Another method involves formation of the metastable $\beta$ phase by rapid solidification and cooling during splat cooling [18, 19], which has resulted in samples with broad $T_c$'s ranging from 6 to 17 K. Solidification rates equal to or exceeding those achieved in splat cooling [20] have been reported [14] for heavily undercooled Nb drops with typical dentrite tip velocities exceeding 300 m/s. Also, it has been shown [2] that metastable phases can be formed by rapid solidification after large amounts of undercooling. Therefore, it could be expected that the high $T_c$ $\beta$ phase of

$Nb_3Ge$ could be formed in bulk samples by rapid solidification of heavily undercooled samples. As will be shown in this study, the metastable $\beta$ phase has been formed after undercooling samples by 300 K.

## II. EXPERIMENTAL TECHNIQUE

The drop tube used for this is a 32 m facility at the Marshall Space Flight Center in Huntsville, Alabama [21]. A schematic of the drop tube is shown in Figure 1. The drop tube consists of a 32 m long, 11 cm diameter, stainless steel tube with a vacuum bell jar located directly atop the tube. The bell jar and tube are evacuated by the two turbomolecular high vacuum pumps. Various instrumentation ports ($I_1$ - $I_6$) and view ports ($VP_1$ - $VP_6$) are located on each floor so that the falling drop may be monitored both optically and electrically. Electropneumatic ($EV_1$ and $EV_2$) and hand-operated vacuum valves ($V_1$ - $V_3$) maintain the vacuum conditions during sample retrieval or insertion of a new sample. Also, an inert gas, such as helium, can be backfilled into the tube to provide for enhanced cooling of low-temperature metals and alloys. When the drop reaches the catcher, it is caught by either a thin foil or a layer of quenching oil, such as a low vapor pressure diffusion pump oil.

The bell jar houses a high-temperature electron bombardment furnace which has also been used as a high-temperature containerless calorimeter [22, 23]. The drop tube can accommodate any furnace which can be adapted to the bell jar. A schematic of the melting apparatus is shown in Figure 2. This furnace employs a heated tungsten filament which emits electrons by thermionic emission. Since the filament is held at negative 5 kV potential, the emitted electrons will bombard and therefore heat the grounded sample. The sample is grounded through the support wire which is, in turn, grounded through a 10 ohm standard resistor. The current striking the sample can then be monitored by measuring the voltage drop across the 10 ohm resistor. The equipotential and focusing grid help to contain and focus the electrons onto the sample.

The sample can be in the form of either a disk, rod, or wire. If the sample is in the form of a wire, it is supported from the support arm, which can be raised or lowered through the gear box which is controlled manually with a rotatable vacuum feedthrough.

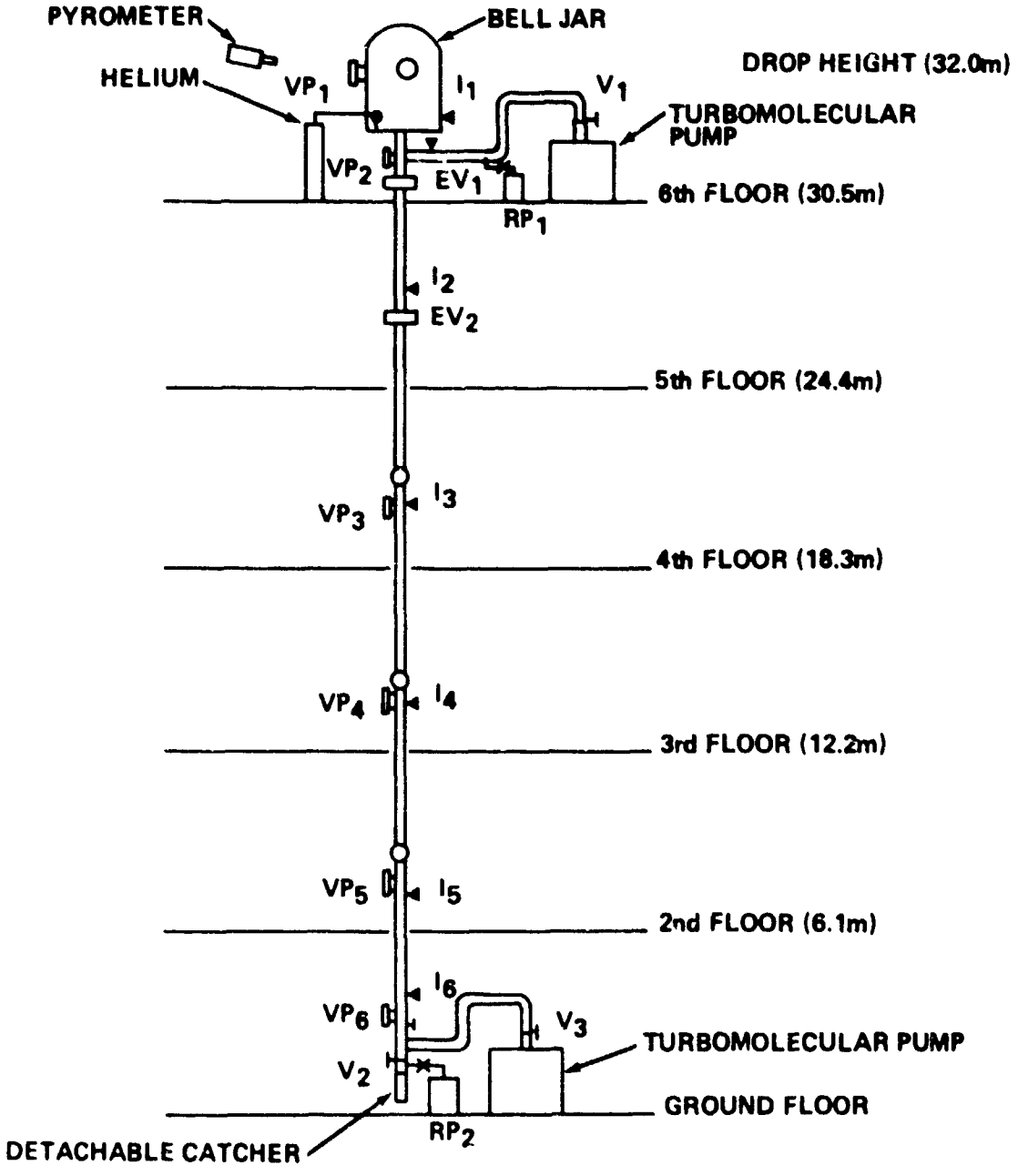


Figure 1. Drop tube diagram.

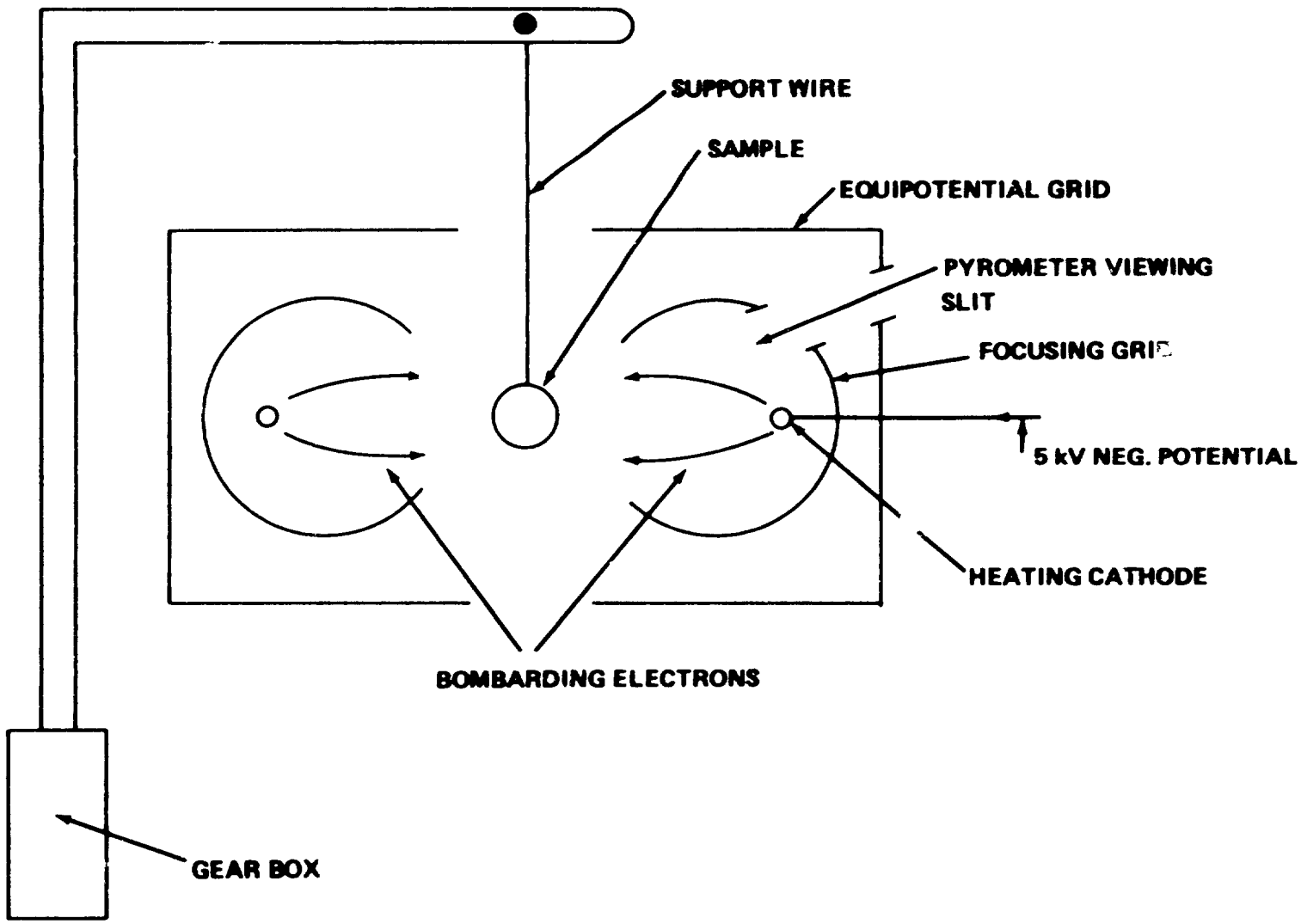


Figure 2. Melting apparatus diagram.

The wire is lowered into the melting apparatus and the filament current increased until melting begins. The wire is then lowered and melted continuously, with the molten material forming a drop clinging to the end of the wire by surface tension. The melting continues until the molten drop becomes too large for the surface tension to hold the drop on the wire. At this point, the molten drop will fall and cool during free fall in the tube.

If the sample is in the form of a disc or half disc, it is suspended from a wire of similar material. For the Nb-Ge alloys a support wire of pure Nb was used. The mass of the disc is selected so that the resulting molten drop will be just slightly less than the mass needed to overcome surface tension and fall. Further heating will overheat the drop above the melting temperature, which decreases the surface tension enough to allow the drop to fall. This method insures the drop is completely molten before falling into the tube.

Since the Nb-Ge alloys were supplied in the form of rods, it was necessary to slice the alloy samples into discs and melt as described previously. To attach the Nb-Ge samples to the support wire, a small hole was drilled through the sample by an electric discharge machine (EDM). A Nb electrode was used to help prevent contamination. The sample was then supported from a hook bent in the end of the support wire. A Nb-Ge alloy sample is shown mounted by this method in Figure 3. The pure Nb samples were both in the form of wires and discs before melting. Before melting, all samples were cleaned for 1 min in hydrofluoric acid and then rinsed with distilled water followed by another rinse with ethyl alcohol.

The instrumentation for the drop tube is shown in block diagram form in Figure 4. The heart of the system is a Hewlett-Packard 9835A desktop computer. The computer controls the plotter, printer, high-resolution digital voltmeter, fast digital volmeter, and the 19-channel scanner. The scanner connects one of the 19 input channels to either of the digital voltmeters which take voltage readings that are stored in the memory of the computer. After a test, all information is stored on a magnetic tape cassette for future reference. Immediately prior to and directly after a drop is made, the vacuum level is measured in the bell jar and in the lower section of the tube. The vacuum gauges use Bayert-Alpert gauge tubes as the measuring sensors.

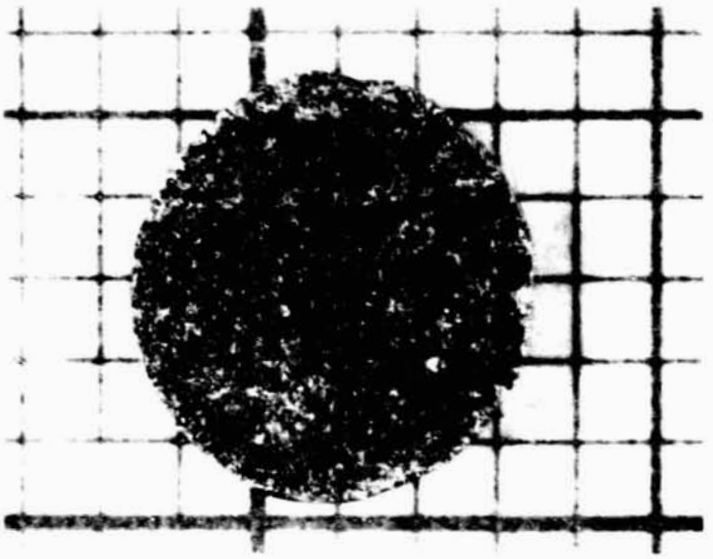

(A) UNMOUNTED SAMPLE WITH HOLE DRILLED FOR MOUNTING

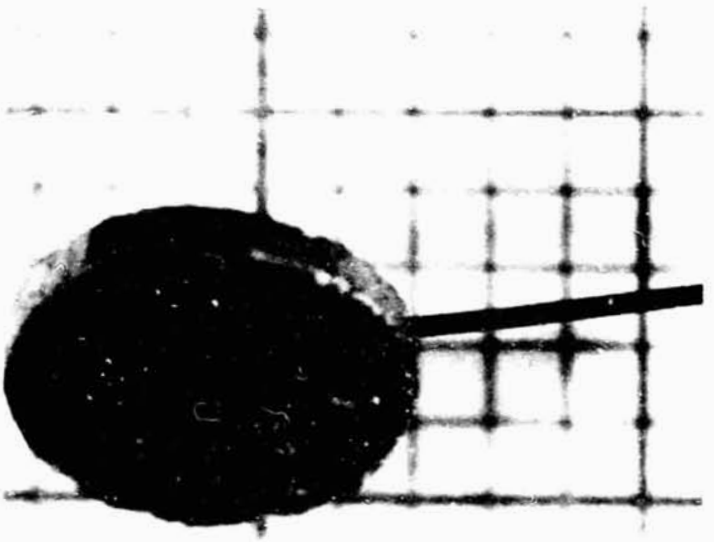

(B) MOUNTED Nb–Ge SAMPLE

Figure 3. Mounting of Nb-Ge samples for melting.

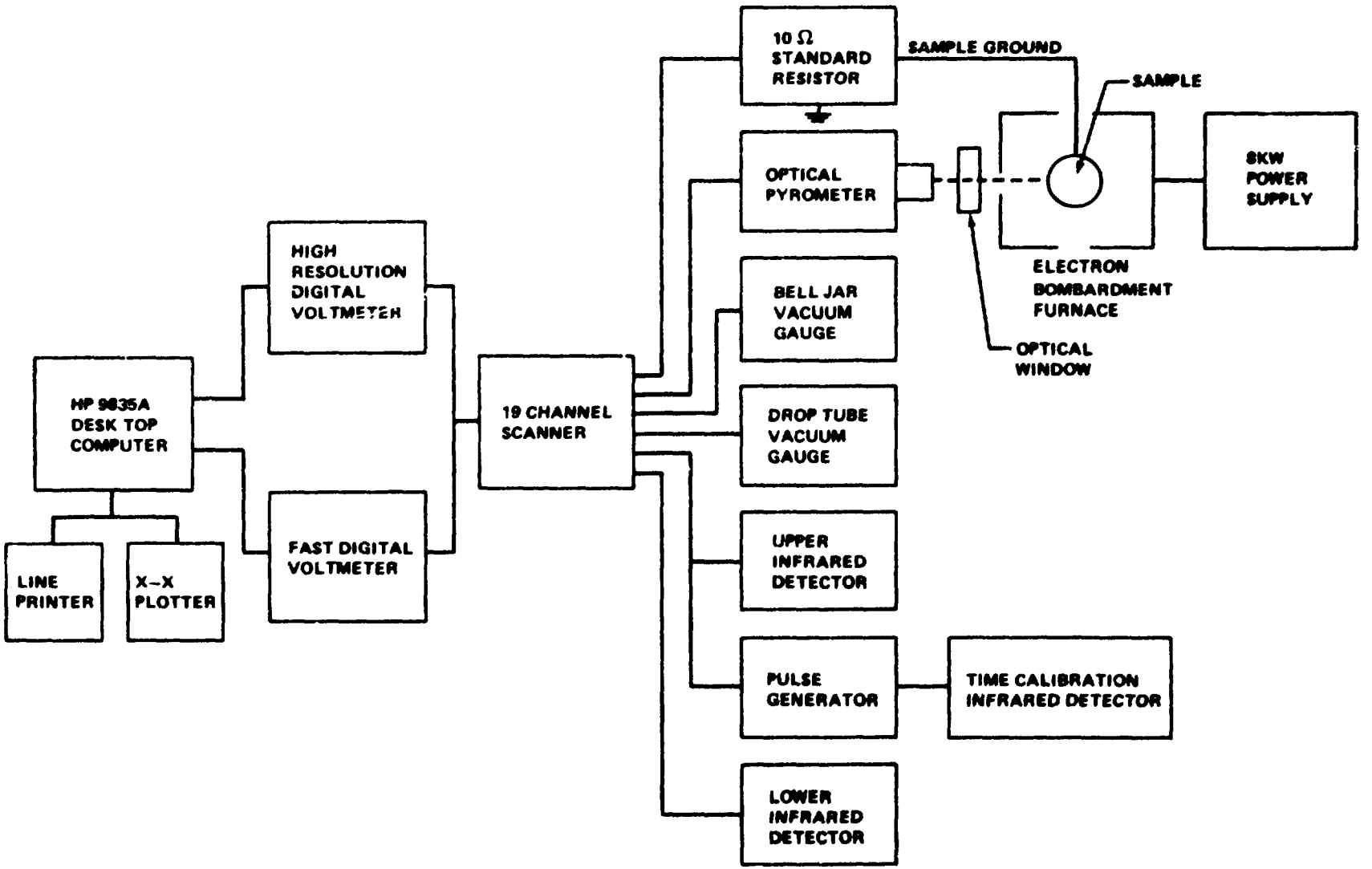


Figure 4. Drop tube instrumentation.

During heating and melting, the sample temperature is measured by an automatic optical pyrometer. The pyrometer measures the actual brightness temperatuure, $T_B$, of the sample; this measurement can be converted to true temperature, $T_t$, by

$$\frac{1}{T_t} = \frac{1}{T_B} + \frac{\lambda}{C_2} \ln \epsilon_s \,, \tag{1}$$

where $C_2$ is a constant equal to 1.43 cm-K, $\lambda$ is the effective wavelength of the pyrometer equal to 0.65 $\mu$m, and $\epsilon_s$ is the spectral emissivity of the sample material. The spectral emissivity of the Nb-Ge was assumed to be the same as the value of 0.317 for pure niobium. This assumption should be valid since the loss of any Ge during the melting will result in a thin layer of mostly Nb on the surface on the drop. The alloy drops would thus be expected to have a spectral emissivity very smiilar to pure Nb. The pyrometer has been calibrated in terms of brightness temperature by the use of a tungsten filament which has been calibrated directly by the National Bureau of Standards. Measured brightness temperatures are therefore accurate to within 0.5 percent. Also, corrections are made for the bell jar optical window to the measured brightness temperatures. The optical pyrometer supplies a voltage through a recorder output which is calibrated with respect to brightness temperature. The pyrometer output voltage is measured by the high-resolution voltmeter and converted to the true sample temperature by the computer.

Also, during heating and melting, the power input into the sample is measured and recorded. The power is the product of the voltage drop from the filament to the sample and the current flowing through the sample to ground. Since the filament potential is held constant during a test, it is only necessary to measure the sample current to know the power input to the sample. A sample current measurement and a sample temperature measurement together with a time measurement from the computer's internal clock are made once every 200 ms. In Figure 5, a typical sample power curve and thermal history are shown for a Nb-Ge alloy disc. Notice that the power and temperature both increase fairly smoothly

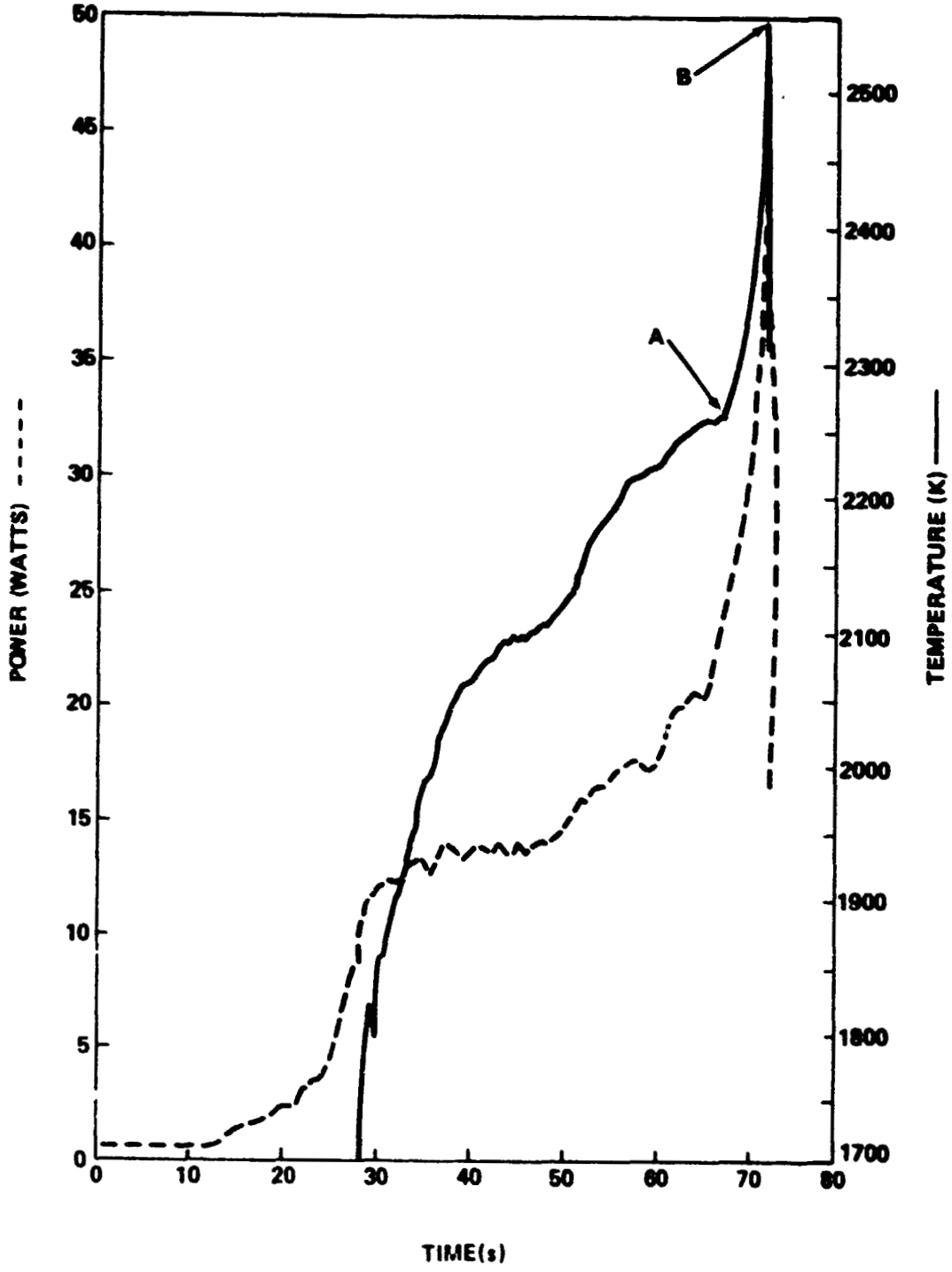


Figure 5. Typical sample heating power and thermal history curves for Nb-Ge alloy sample.

until point A, which corresponds to the time at which the sample was completely molten and formed a spherical drop. The power and temperature then increase very rapidly until the drop falls at point B.

During free fall, the brightness of the drop is monitored by the upper and lower infrared detectors. The detectors used for this study are two silicon photovoltaic detectors produced by United Detector Technology (Model # UDT-450). These detectors incorporate an operational amplifier built into the TO-5 case containing the silicon chip and are sensitive to light in the range of 0.3 to 1.1 $\mu$m. An electrical diagram of the detector and amplifire is shown in Figure 6. Also, the output voltage versus input light intensity is shown in Figure 7. During this study the feedback resistor $R_f$ was set at 10 mega-ohms so that, as can be seen from Figure 7, the detectors were sensitive to light intensities from $10^{-5}$ to $10^{-11}$ W/cm$^2$. The detectors were mounted as shown in Figure 8 with the upper detector located just below the bell jar looking down and the lower detector located slightly above the catcher looking up. The detectors are mounted so as to exploit the large field of view of the detector so that the drop can be monitored everywhere in the tube with the exception of the first 20 cm of free fall.

The output voltage from the detectors may either be recorded on a fast strip chart recorder or stored by the computer. By referring to Figure 5, it can be seen that when the drop falls, the sample current decreases very sharply. This sudden decrease is used to trigger the computer to switch the scanner to the upper infrared detector and to begin taking readings through the fast digital voltmeter. Readings are normally taken at a rate of 4000/s. After the drop has fallen for 1.5 s, the scanner can be switched to the lower infrared detector if desired. This would be necessary in the case of low-temperature drops since the lower detector is closer to the drop while falling in the second half of the tube. However, the upper detector proved adequate for monitoring the brightness of the Nb and Nb-Ge drops everywhere in the tube. Therefore, the bottom detector was used just to provide redundant information.

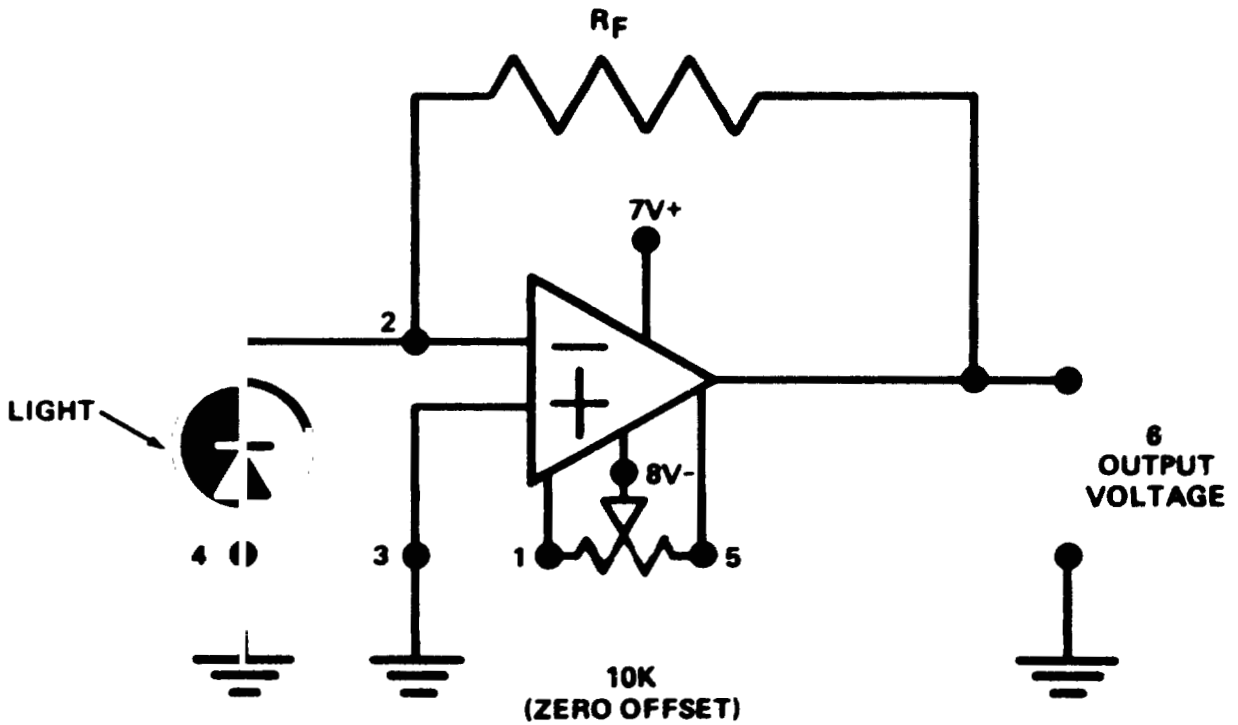


Figure 6. Electrical diagram of infrared detector and amplifier.

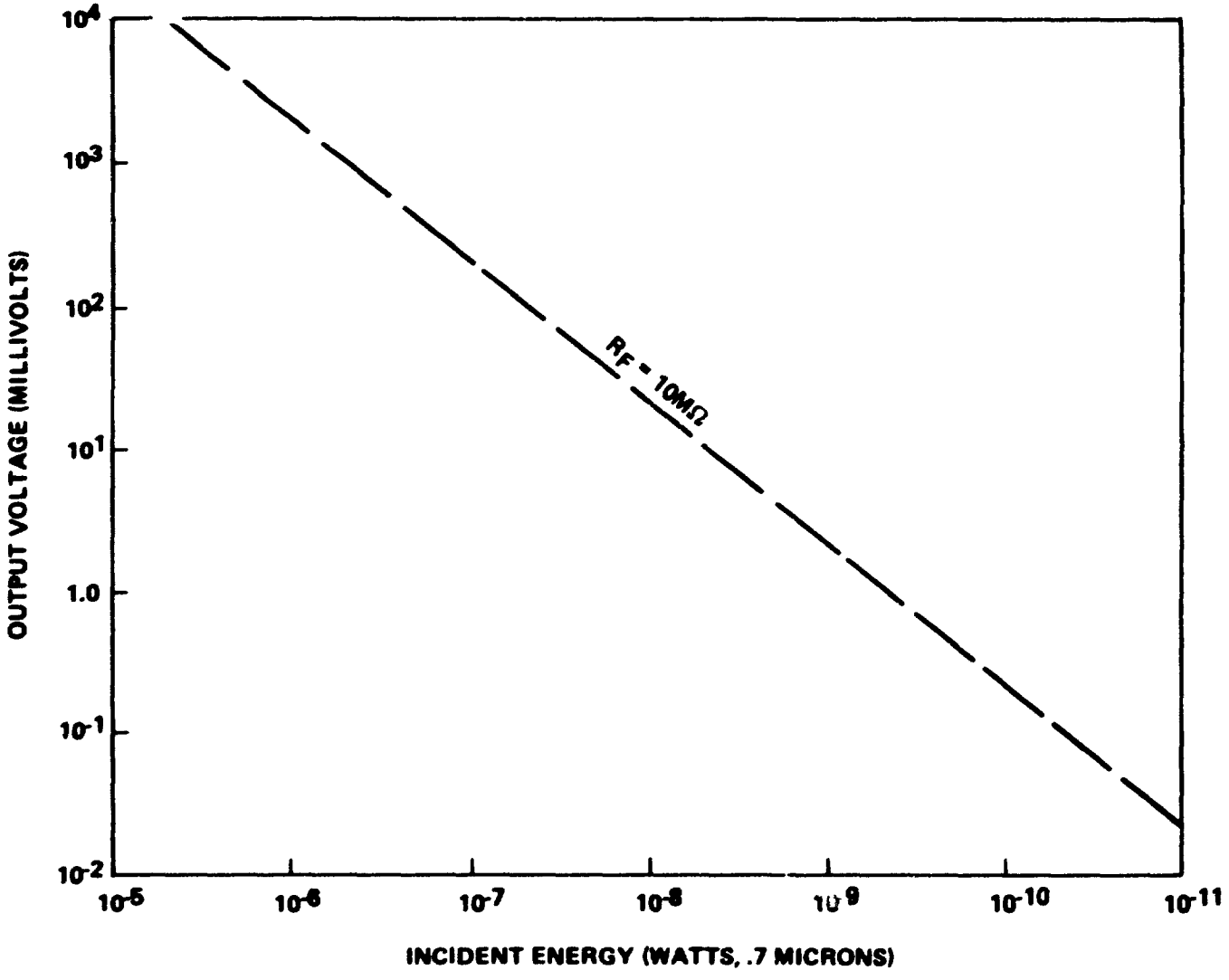


Figure 7. Output voltage versus incident light energy for infrared detector.

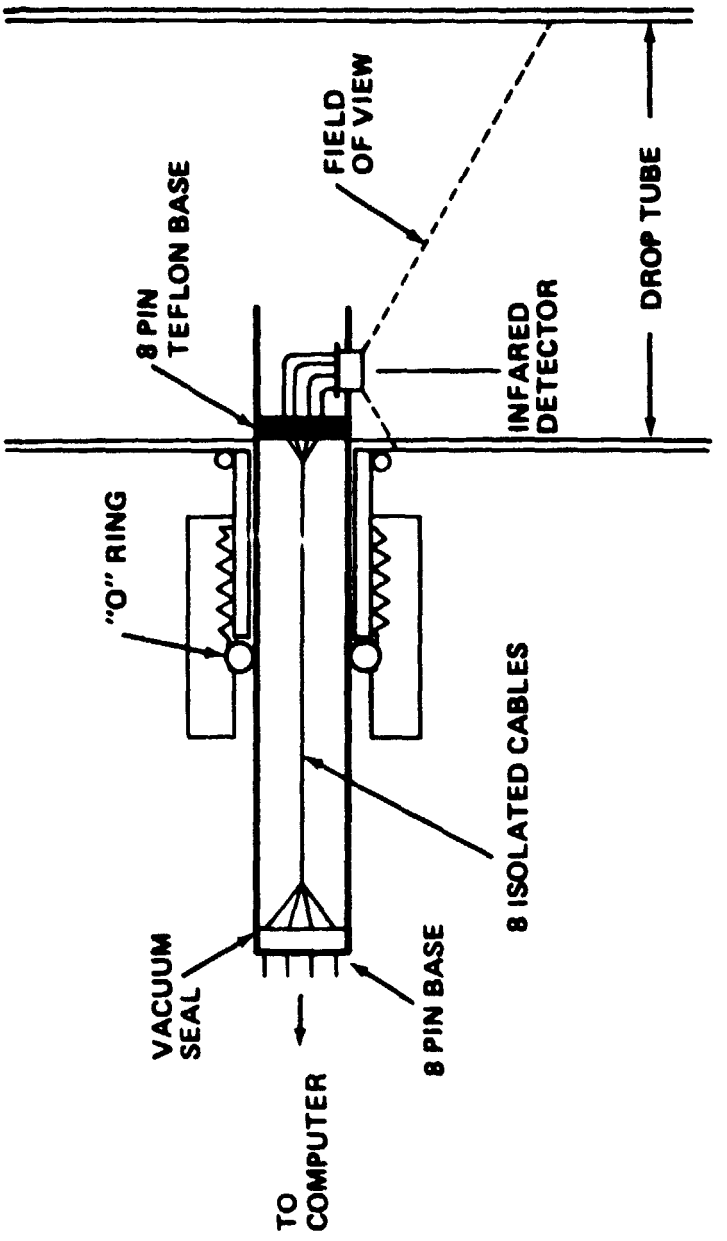


Figure 8. Infrared detector mounting.

As the drop falls, it will cool due to heat loss by radiation. The rate of heat loss $\dot{Q}_R$ will be given by the Boltzmann radiation law [24] for the sphere in a vacuum:

$$\dot{Q}_R = \frac{dQ_R}{dt} = -\epsilon_T A\sigma(T^4 - T_0^4) \quad . \tag{2}$$

In equation (2), $\epsilon_T$ is the total hemispherical emissivity, A the surface area of the drop, $\sigma$ the Boltzmann's constant, T the temperature of the sphere, and $T_0$ the ambient temperature. Once the undercooled drop nucleates and crystal growth begins, the temperature of the drop will increase very rapidly. This recalescence appears as a sudden increase in the brightness of the drop over the radiation $\dot{Q}_N$ emitted at the nucleation temperature $T_N$. Differentiating and normalizing equation (2), yields:

$$\frac{\Delta\dot{Q}}{\dot{Q}_N} \cong \frac{4\,\Delta T}{T_N} \tag{3}$$

where $\Delta T$ is the increase in temperature due to recalescence and $\Delta\dot{Q}$ the increase in brightness. From equation (3), it can be seen that a 1 percent increase in sample temperature would give a 4 percent increase in drop brightness. This increase in brightness can be detected by the infrared detectors.

In Figure 9, the output of the upper infrared detector during three pure niobium drops is compared (Curves A, B, and C) as recorded on a strip chart recorder. Curve D of Figure 9 is a sample current trace for a drop formed from a Nb wire and is included to show the decrease in sample current, denoted by point 1, corresponding to the time of drop release. Curve A is a detector output for a Nb drop that did not undercool. Curves B and C are typical detector signals for 3 and 5 mm diameter Nb drops, respectively, which both undercooled 530 K. Notice the sharp recalescence peaks denoted by point 3 which is absent in curve A. The recalescence peak is different for the two drops due to the fact that the cooling rate is size dependent, as will be shown in Section III. Thus, the recalescence peak can be detected and recorded. Point 2 denotes a common peak in Curves A, B, and C which corresponds to the time when the drop first comes into the field of view of the upper detector.

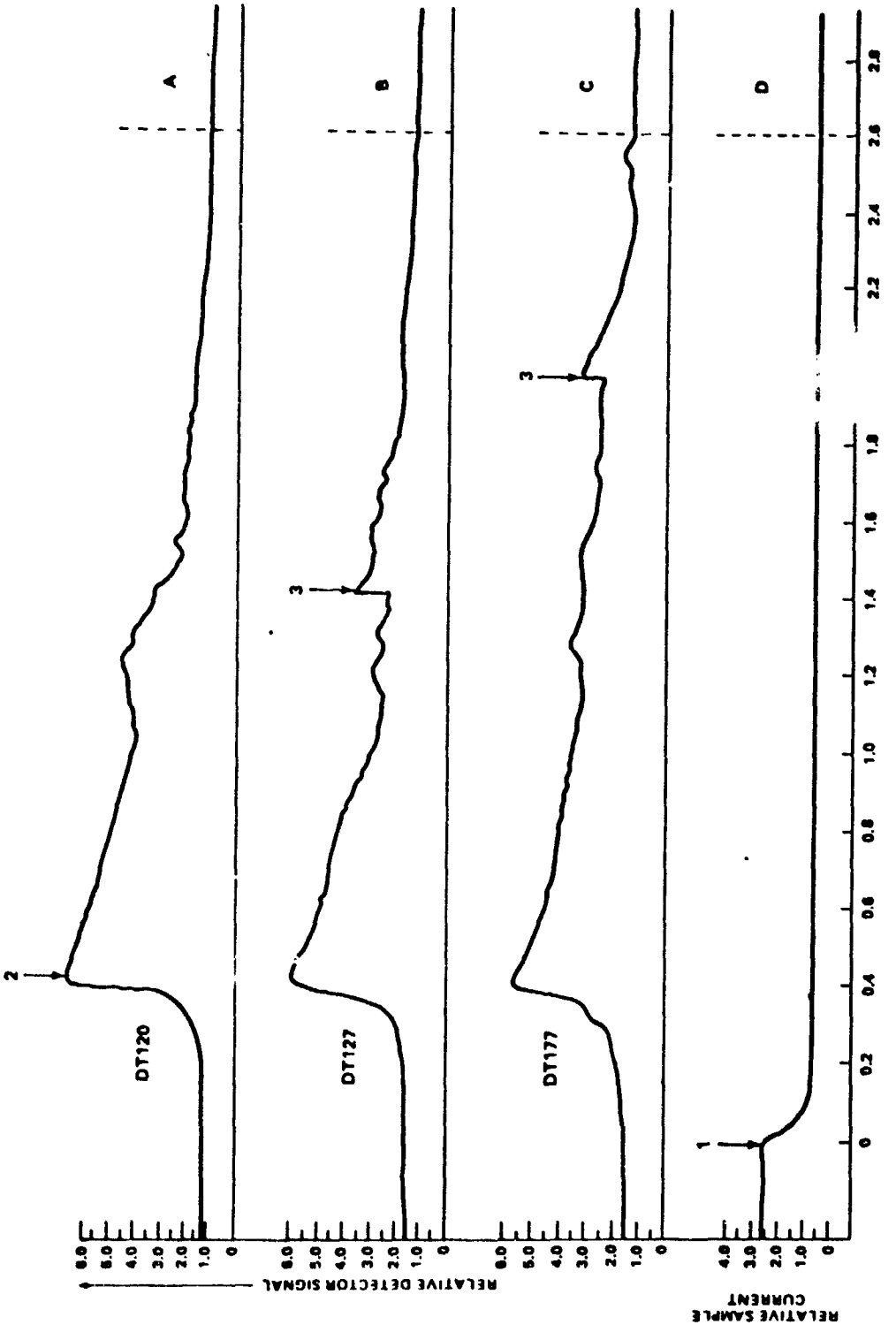


Figure 9. Typical infrared detector output for Nb drops.

When the detector output is stored on the computer, there exists a problem of calibrating the detector output, and therefore the recalescence peak time, with the absolute time of drop release. The problem originates from the fact that, although the fast digital voltmeter takes readings at precisely 4000 readings per second, there exists an uncertainty of as much as 200 ms as to when the scanner switched and the fast voltmeter was triggered to begin taking data. This problem has been solved by the use of the time calibration infrared detector. This detector is the same type as the detectors which monitor the brightness of the drop but has a very small field of view limited by a narrow tube. Therefore, the time calibration detector can only "see" the drop when the drop is directly in front of it. Therefore, the peak of the output of the time calibration detector corresponds to the time at which the drop was exactly at the detector position in the drop tube. The distance of free fall to the time calibration detector has been measured to be 30.45 m and thus corresponds to a free-fall time of 2.493 s since the acceleration due to gravity is constant and is known to be 979.6362 $cm/s^2$ [25]. The signal from the time calibration detector is fed into a pulse generator with an adjustable trigger. When the drop is detected, the pulse generator is triggered and instantaneously outputs a narrow 500 $\mu s$ pulse onto the signal of the upper infrared detector which monitors the brightness of the drop. The sharp pulse that appears on the upper infrared detector trace corresponds to a precisely known ($\pm$ 1 ms) freefall time. All other points can then be referenced to this time calibration peak and are, therefore, also known accurately in terms of actual free-fall time. Thus, the time of free-fall and cooling before recalescence can be measured to an accuracy of 1 ms, which corresponds to determining the position of the drop within the tube during recalescence to within 1 cm.

In figure 10, an upper infrared detector signal, as stored by the computer, is shown for a Nb-22 a/o Ge alloy drop which undercooled all the way down the tube and recalesced upon entering the quenching oil in the catcher. Recalescence is denoted by point 1, while the time calibration peak is shown as point 2. Since the information in Figure 10 is stored on the magnetic tape cassette, it can be recalled and replotted in many different ways. In

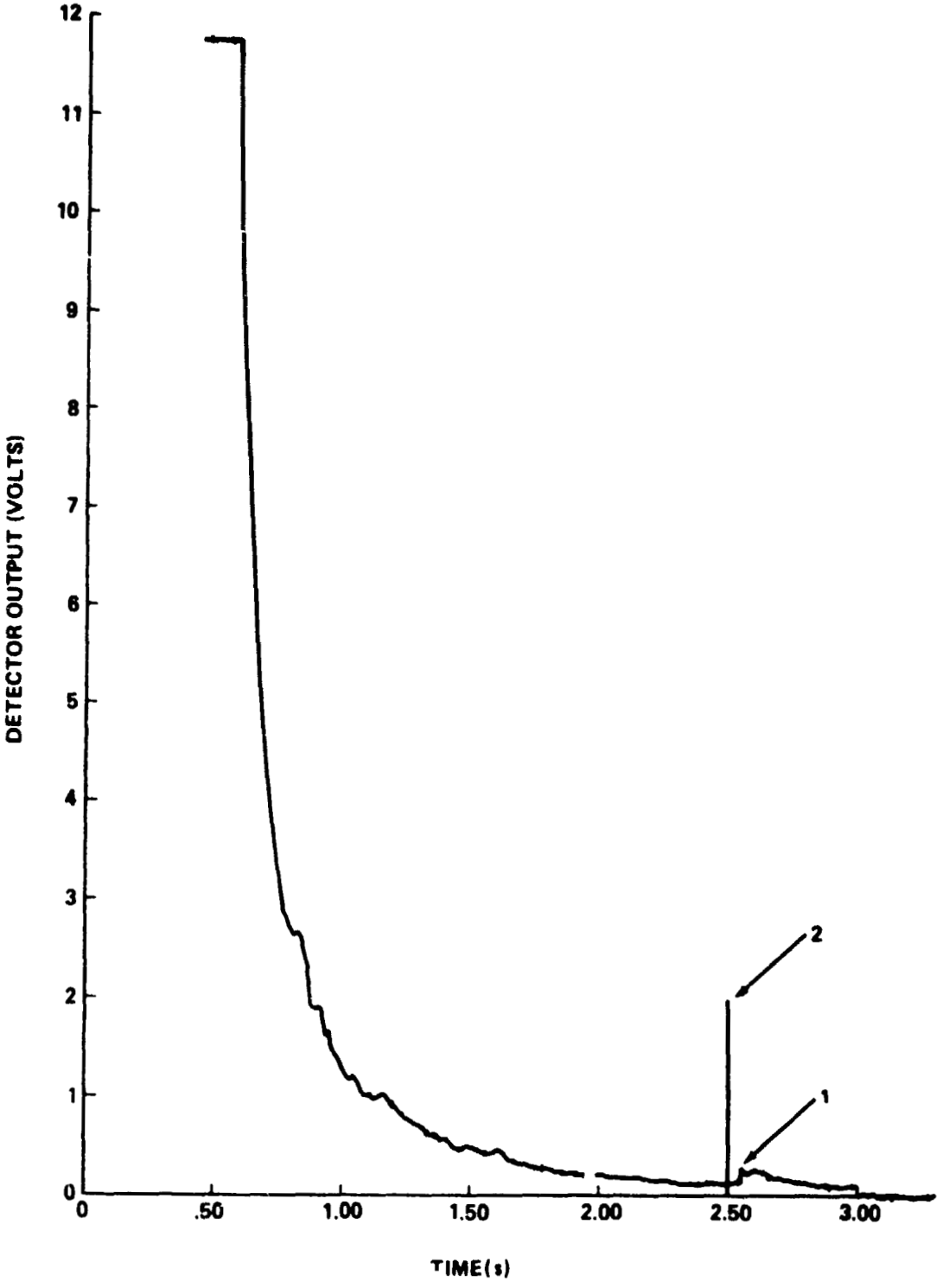


Figure 10. Compu'er-stored infrared detector signal for Nb-Ge alloy drop.

Figure 11, only a small portion of the overall trace is reproduced in an expanded scale. Notice the recalescence peak is now very easy to detect and much greater than the residual noise. This allows detailed analysis of the shape and time of the recalescence peak and illustrates the value of storing the data with the computer.

Since the time of occurrence for the recalescence peak is known very accurately, the amount of undercooling can then be measured if the cooling curve for the drop is known. The next section is dedicated to the analysis of the cooling curves for the Nb and Nb-Ge alloy drops.

## III. THEORY

If a drop is falling in a vacuum, it will lose heat only by radiation and at the rate described in equation (2). The effect on the radiation heat loss by reflection of energy back onto the drop by the drop tube walls is discussed in Appendix A and is found to be negligible. Also, the heat lost by evaporation is found to be small (Appendix B). If the drop does not undercool, it will begin to solidify when the temperature decreases to the melting point. During solidification the temperature of the drop will remain constant at the melting temperature. The time of solidification, $t_s$, can then be deduced from equation (2) to be:

$$t_s = m H_f / |\epsilon_T A\sigma (T_m^4 - T_0^4)| \quad , \tag{4}$$

where m is the mass of the drop and $H_f$ is the heat of fusion. From equation (4) and the thermophysical properties of Nb given in Table 1, it can be calculated that the maximum size Nb drop that can be completely solidified in the drop tube is 5 mm in diameter. This drop size has been successfully prepared in the drop tube.

If the drop does not solidify upon release, it will undercool. In this event, $\dot{Q}_R$ of equation (2) will be

$$\dot{Q} = mC \frac{dT}{dt} \quad , \tag{5}$$

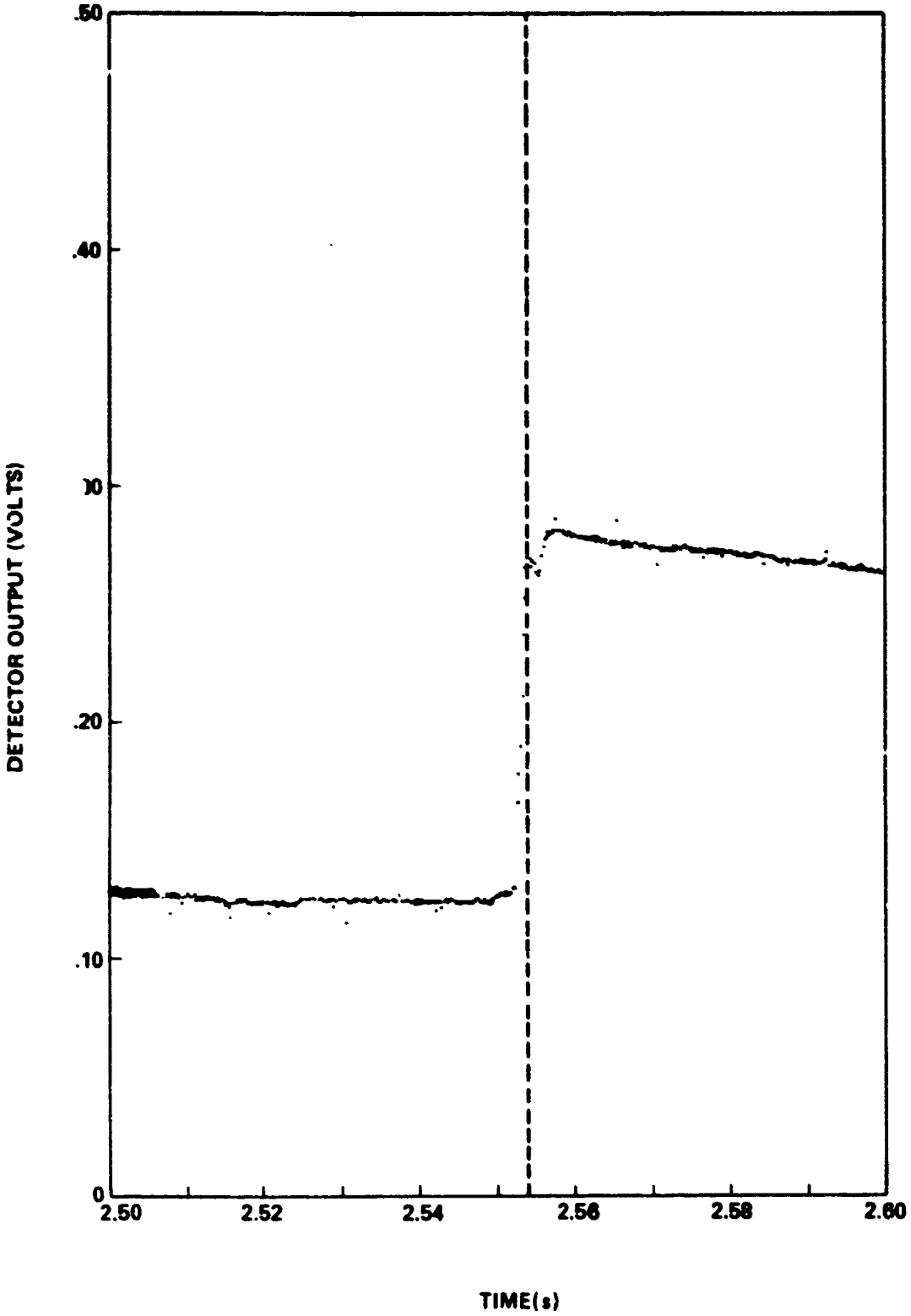


Figure 11. Expanded recalescence peak for Nb-Ge alloy drop.

TABLE 1

THERMOPHYSICAL PROPERTIES

| | Nb | Nb-13 a/o Ge | Nb-18 a/o Ge | Nb-22 a/o Ge | Reference |
|---|---|---|---|---|---|
| Heat of Fusion (J/kg) | $2.88 \times 10^5$ | - | - | - | 26, 27 |
| Melting Temperature (K) | 2741 | 2517 | 2337 | 2173 | 28, 29 |
| Solid Specific Heat (J/kg-K) | 440 | - | - | - | 26 |
| | 410 | 356 | 368 | 398 | (This study) |
| Liquid Specific Heat (J/kg-K) | 435 | - | - | - | 31 |
| | - | - | 398 | 398 | (This study) |
| Spectral Emissivity | 0.317 | 0.317 | 0.317 | 0.317 | 30 |
| Total Hemispherical Emissivity at $T_m$ | 0.310 | - | - | - | 26 |
| | | 0.298 | 0.295 | 0.271 | (This study) |

where C is the specific heat of the material. Equation (2) then reduces to:

$$\frac{dT}{dt} = -K_o(T^4 - R_o^4) \quad , \tag{6}$$

where

$$K_o = \frac{\epsilon_T A\sigma}{mC} \quad .$$

Equation (5) can then be integrated to yield

$$t_c = \frac{1}{4K_oT_o^3} \left[ \ln \frac{(T + T_o)}{T - T_o} + 2 \tan^{-1} \left(\frac{T}{T_o}\right)\right] + \text{constant} \tag{7}$$

by assuming the drop to be isothermal during cooling and a temperature independence in $K_o$. The validity of assuming isothermal cooling has been addressed [32], with the result that the gradient within the liquid sample should be less than 20 K in a 4 mm drop of Nb or 0.7 percent of the melting temperature and even less for the Nb-Ge alloys. The time, $t_c$, in equation (6) is the time necessary for a drop to cool from some initial temperature, $T_i$, to the final temperature, $T_f$. The constant is evaluated at $T = T_i$ and $t_c = 0$. Also in the derivation of equation (6), it was assumed that the material parameters are constant while cooling from $T_i$ to $T_f$. While the surface area A and drop mass m can be considered constant over a wide range of temperature, the total emissivity $\epsilon_T$ and the specific heat C vary with temperature. However, if the temperature difference from $T_i$ to $T_f$ is taken in small increments, $\Delta T_j$, of the total cooling $\Delta T$, then $\epsilon_T$ and C are essentially constant over the small temperature difference $\Delta T_j$, and equation (6) can be applied. To calculate the total cooling time $t_c$ over a wide temperature range, the cooling time $t_{cj}$ for each increment $\Delta T_j$ of temperature can be summed:

$$t_c = \sum_{j}^{N} t_{cj} \quad . \tag{8}$$

where each $t_{cj}$ is calculated from equation (6) for the temperature increment $\Delta T_j$, with $\epsilon_T$ and C being adjusted for each temperature increment.

Since the optical pyrometer measures the temperature of the drop at the time of release, $T_i$ is known and a cooling curve for each drop can be calculated once the thermophysical properties are known. By using the parameters for Nb given in Table 1, the undercooling curves for pure Nb have been calculated and are presented in Figure 12 for various drop diameters. Once the cooling curves are calculated and the time of recalescence has been measured by the infrared detectors, it is a simple matter to determine the amount of cooling $\Delta T_c$ before recalescence. Since the Nb-Ge alloy drops are usually overheated above the melting point before release, the overheating $T_{ov}$ must be subtracted from the total amount of cooling $\Delta T_c$ to give the actual amount of undercooling $T_u$. For Nb, there is little or no overheating so that the drop is at the melting temperature upon release and begins to undercool immediately.

## IV. HIGH-TEMPERATURE CALORIMETRY

As stated previously, the furnace used for this study is actually a high-temperature, containerless calorimeter [22, 23]. Since the emissivity and specific heats of the Nb-Ge alloys were not known, it was necessary to measure these parameters using the calorimeter. To do this a sample material would be completely melted and allowed to solidify while still clinging to the support wire. Due to the high surface tension of these metals, the resulting droplet was essentially spherical to within 1.5 percent accuracy. Therefore, upon cooling, a drop attached to the support wire can be treated as a sphere cooling by radiation with a correction for the heat loss due to the support wire: The heat loss due to the wire, $\dot{Q}_w$ is found in Appendix C to be:

$$\dot{Q}_w = -\pi(\epsilon_w \sigma T^5 K R_w^3)^{1/2} \tag{9}$$

where $\epsilon_w$, K, and $R_w$ are, respectively, the emissivity, thermal conductivity, and radius of the support wire. T is again the temperature of the drop. Generally the heat loss because of the wire was approximately 10 percent or less of the total heat loss of the sphere.

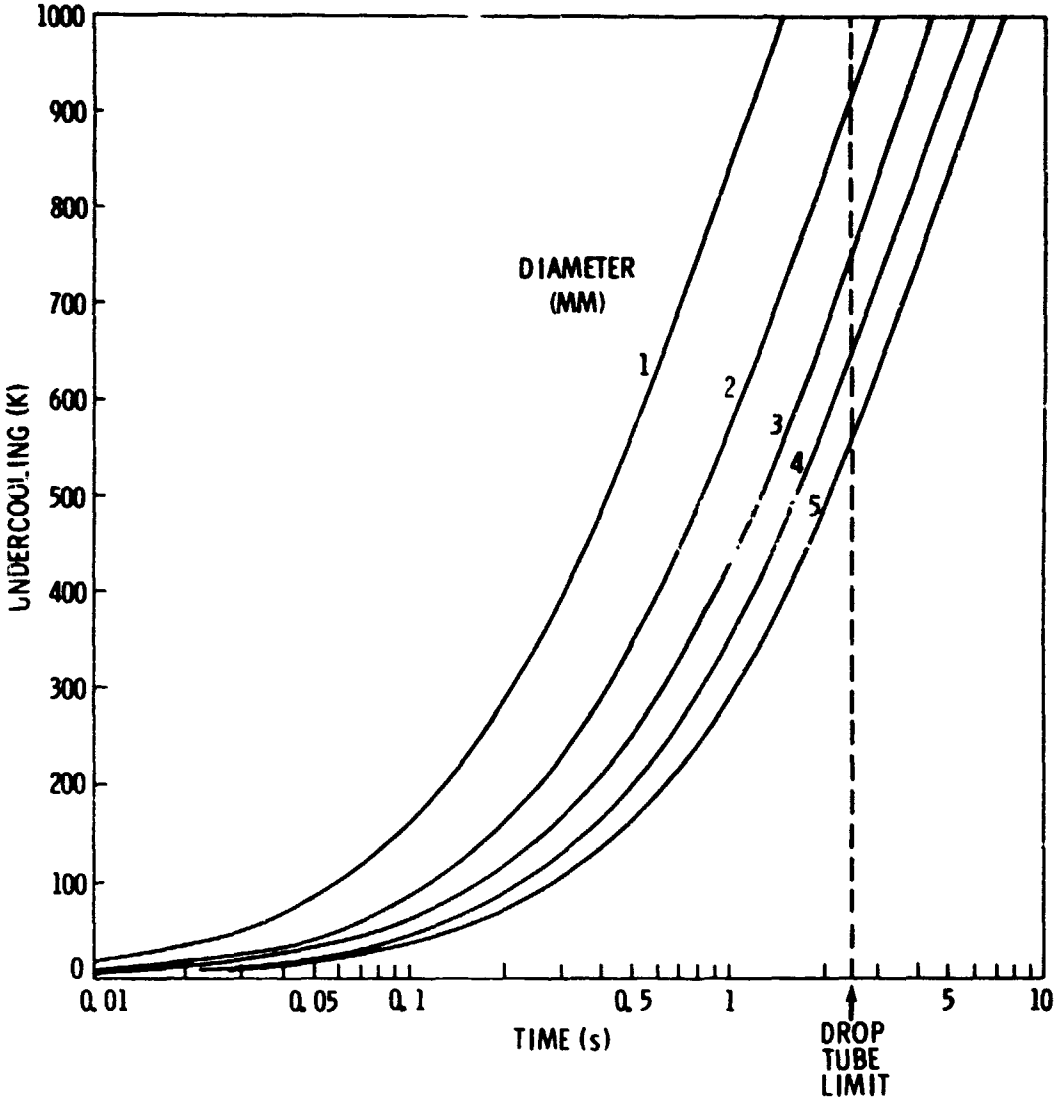


Figure 12. Undercooling curves for various diameter Nb drops.

When the spherical sample is re-heated and held at a constant temperature, the heat input into the sample must equal the heat loss by the sample. Since the heat input, $\dot{Q}_I$, into the sample is measured as described in Section II, the total hemispherical emissivity can be calculated by equating $\dot{Q}_I$ to the heat loss by radiation $\dot{Q}_R$, with the connection for the heat loss due to the wire $\dot{Q}_W$:

$$\dot{Q}_I = \dot{Q}_R + \dot{Q}_W \tag{10}$$

Plugging in for $\dot{Q}_W$ from equation (8) and $\dot{Q}_R$ from equation (2) yields:

$$\dot{Q}_I = -\epsilon_T A\sigma(T^4 - T_o^4) - \pi(\epsilon_W \sigma T^5 K R_W^3)^{1/2} \quad . \tag{11}$$

For the calorimetry studies a support wire of tungsten, which has known properties [28], was used. Since the properties of tungsten are known, the only unknown in equation (10) is the total hemispherical emissivity, $\epsilon_T$, of the sample droplet. Using the computer, equation (10) can be solved for $\epsilon_T$ and repeated for many different points. Each measured emissivity is therefore a statistical average of 50 to 100 measurements, with the typical standard deviation being less than 0.5 percent. Emissivity measurements were thus made for Nb and the Nb-Ge alloys over a wide temperature range and are presented in Figure 13. The solid line in Figure 13 is an experimental literature curve for pure Nb [26]. As can be seen, the agreement between this study and the published curve for Nb is fairly close. Also, notice that the Nb-Ge alloys appear to have emissivities very similar to pure Nb. Thus, it appears justifiable to use the total hemispherical emissivity values for Nb for cooling calculations involving the Nb-Ge alloys for compositions, at least up to 22 a/o Ge. For this study the values of emissivity for both Nb and the Nb-Ge alloys were therefore assumed to be [26]:

$$\epsilon_T = -0.144 + 2.88 \times 10^{-4} T - 4.46 \times 10^{-8} T^2 \quad . \tag{12}$$

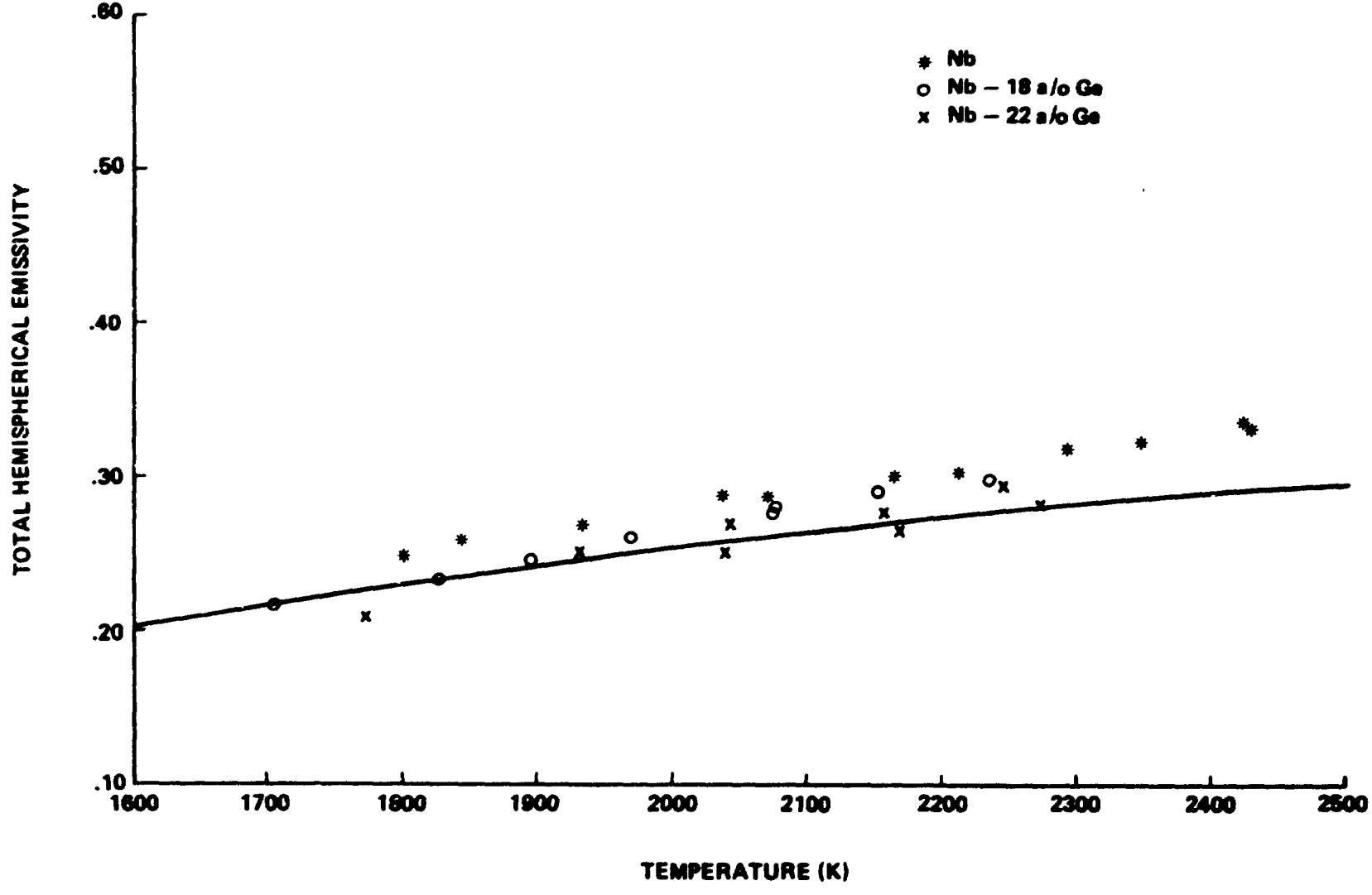


Figure 13. Measured total emissivities for pure Nb and Nb-Ge alloys compared to literature curve (solid line) for pure Nb.

Although the total emissivities discussed to this point are for solid Nb and Nb-Ge alloys, it will be assumed in this study that the emissivity curve of equation (11) also describes the total emissivities of these materials in the undercooled liquid state. This assumption is necessary because of the total absence of published liquid total emissivity values for Nb and Nb-Ge alloys and the technical complexity of measuring the total emissivities for such high-temperature materials in the undercooled state.

The specific heats of Nb and the Nb-Ge alloys were measured by reheating the spherical drop, still attached to the support wire, to near its melting temperature and then cutting off the power to the tungsten filament. The temperature of the sample was then recorded as it cooled. Since during cooling there is no heat input, the drop will simply cool by radiation with some heat loss up the wire so that

$$\dot{Q} = \dot{Q}_R + \dot{Q}_w \tag{13}$$

which reduces to

$$mC\frac{dT}{dt} = -\epsilon_T A\sigma(T^4 - T_o^4) - \pi(\epsilon_w \sigma T^5 K R_w^3)^{1/2} \tag{14}$$

by use of equations (2), (5), and (8). The only unknown in equation (13) will be the specific heat C once the cooling curve for the sample has been measured. Figure 14 shows the cooling data for a Nb droplet together with a calculated cooling curve from equation (13) using the constant value of 410 J/kg-K. Since the specific heat changes slowly with temperature, a constant value of C can be used, with the resulting error being less than 2 percent over the temperature range encountered in this study. The value of 410 J/kg for the specific heat of Nb compares well with literature values [26]. Since there appears to be an agreement between the specific heat of solid Nb [26] near the melting point and liquid Nb [31] just above the melting point, it is believed the specific heat values of solid Nb could be used in undercooling calculations.

The specific heats for the Nb-Ge alloys were also measured in the solid state; the constant C for which the calculated curve most closely fit the raw data is presented in

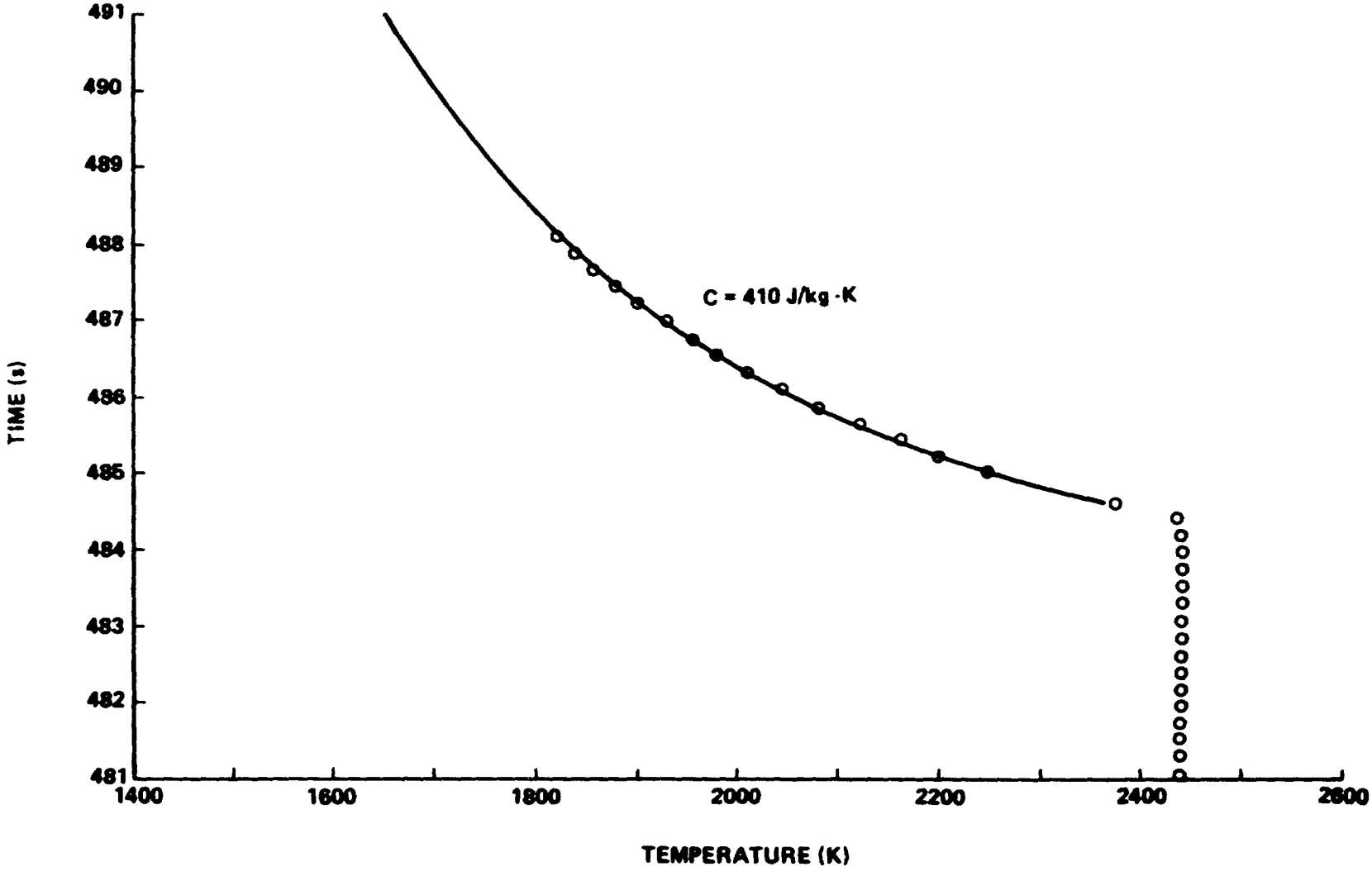


Figure 14. Calculated cooling curve for Nb droplet compared to measured data.

Table 1. A typical measured cooling curve for Nb-18 a/o Ge droplet is shown in Figure 15 and is compared to the calculated cooling curve using the specific heat value of Table 1. Several cooling curves were measured for each composition, with the resulting specific heats being averaged for Table 1. An effort was also made to measure the specific heats of the alloys in the liquid state. Figure 16 shows a measured cooling curve for a Nb-22 a/o Ge droplet which was heated to approximately 300 K above the liquidus temperature before being cooled. In this way the liquid specific heat could be measured near the melting point. As can be seen in Figure 16, the specific heat value of 398 J/kg, which is the average measured specific heat for the solid Nb-22 a/o Ge droplets, also fits the measured cooling curve for the liquid (Curve A) quite well. Curve B of Figure 16 is the measured cooling curve for the same droplet after solidification and is compared to the calculated cooling curve with a C of 390 J/kg. Similar measurements were made for the Nb-18 a/o Ge alloy with the same result that the measured average specific heat for the solid state also compared well with the measured liquid specific heats. As previously noted, the specific heat of solid Nb compares closely to the specific heat of liquid Nb near the melting point. Therefore, it appears justified to use the specific heats of solid Nb and Nb-Ge alloys in cooling calculations for undercooled Nb and Nb-Ge drops. The values of the specific heats presented in Table 1 were thus used for undercooling calculations.

With these measured values the emissivities and specific heats, the cooling curve for any Nb or Nb-Ge drop could be calculated as described in Section III. Thus, once the time of cooling before recalescence was measured by the infrared detectors, the amount of undercooling in terms of temperature was known.

## V. RESULTS

Using the infrared detectors to measure the cooling time before recalescence and the cooling curves calculated as previously described, the amount of undercooling was measured for a number of pure Nb and Nb-Ge alloy drops. The results for some of the Nb drops are presented in Table 2. From Table 2, it can be seen that the Nb drops consistently undercooled 525 K, independent of drop size, before nucleation and recalescence occurred. This amount of undercooling corresponds to 19 percent of the melting temperature of 2741 K for Nb and is, therefore, consistent with the empirical homogeneous nucleation

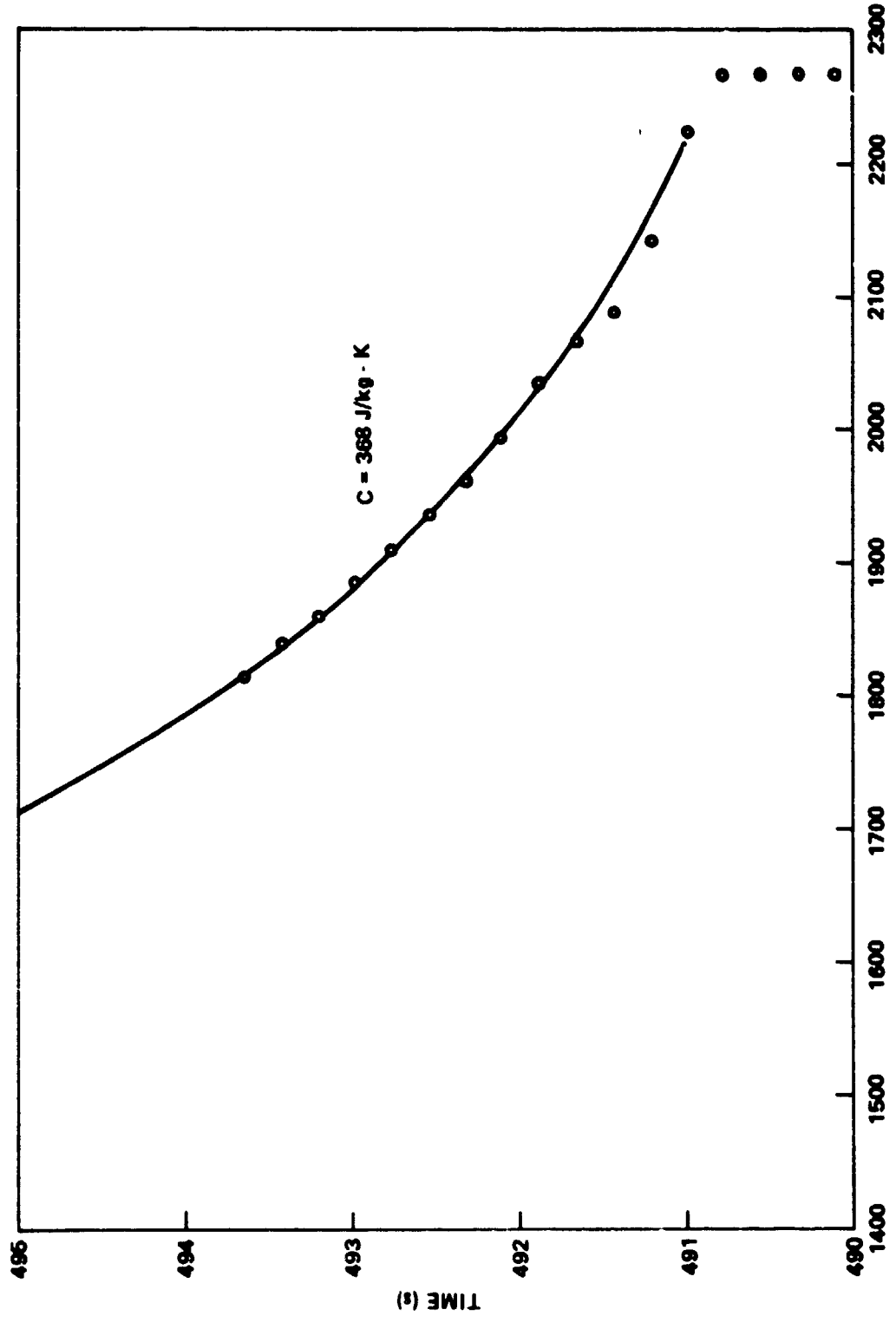


Figure 15. Calculated cooling curve for Nb-18 a/o Ge droplet compared to measured data.

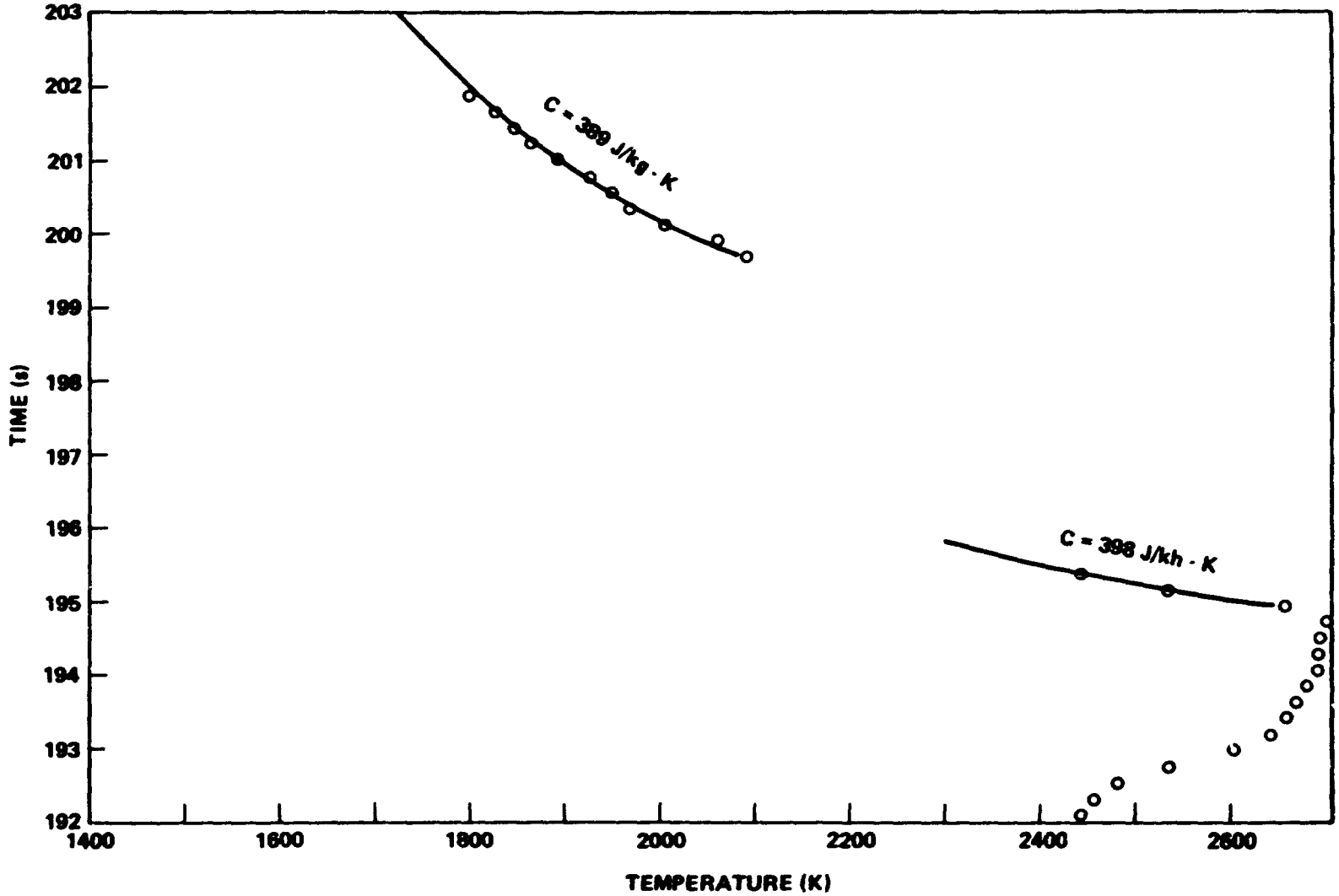


Figure 16. Calculated cooling curves for liquid and solid Nb-22 a/o Ge droplet compared to measured data.

TABLE 2

MEASURED UNDERCOOLING FOR Nb DROPLETS

| Drop Number | Mass (mg) | $T_u$ (K) | $T_u/T_m$ |
|---|---|---|---|
| DT126 | 120.0 | 528 | 0.193 |
| DT127 | 125.2 | 535 | 0.194 |
| DT128 | 120.6 | 532 | 0.194 |
| DT138 | 123.0 | 532 | 0.194 |
| DT125 | 327.1 | 526 | 0.192 |
| DT129 | 332.9 | 531 | 0.194 |
| DT130 | 329.1 | 514 | 0.188 |
| DT131 | 327.8 | 515 | 0.188 |
| DT132 | 312.5 | 524 | 0.191 |
| DT134 | 321.7 | 528 | 0.193 |
| DT135 | 316.3 | 512 | 0.187 |
| DT136 | 294.6 | 520 | 0.190 |
| DT137 | 304.4 | 531 | 0.194 |
| DT139 | 362.3 | 535 | 0.195 |
| DT142 | 364.8 | 517 | 0.189 |
| DT144 | 352.6 | 528 | 0.193 |
| Average | Small Drops | 531 | 0.194 |
| Average | Large Drops | 523 | 0.191 |
| TOTAL AVERAGE | — | 525 ± 8 | 0.192 ± 0.003 |

limit of Turnbull. However, the nucleation temperature ($T_N$ = 2216 K) also corresponds to the reported [33] melting point of NbO at 2218 K. Thus, the results could also be due to heterogeneous nucleation induced by the formation of cubic NbO on the surface of the cooling Nb drop. Drops of Nb were also made that were released with a portion of unmelted Nb wire within the sample. These drops experienced little or no undercooling since the molten Nb would nucleate from the unmolten Nb wire. A comparison between undercooled and not undercooled Nb samples could then be made.

A photomicrograph of a typical undercooled Nb sample is shown in Figure 17A with an X-ray Laue diffraction pattern of this drop included in Figure 17B. All Laue diffraction patterns show only single crystal Nb behavior with no evidence of fine grain polycrystalline behavior as reported by Walker [4] for undercooled Ni. In Figure 18, the surfaces of undercooled and not undercooled samples are compared as photographed by a scanning electron microscope (SEM). Notice that the drop which was not undercooled (Figure 18A) shows a very smooth surface with no distinguishing characteristics. Conversely, the undercooled drop (Figure 18B) shows a distinct "wrinkling" which is believed to be due to interdendritic shrinkage channels.

Differences can also be seen in the interior microstructure of the Nb samples with respect to undercooling. The undercooled samples exhibited [illegible]cture of single crystal behavior, as shown in Figure 19 for a heavily etched Nb sample. A series of Laue diffraction patterns taken across the exposed interior surface confirmed the sample is single crystalline. Samples with little or no undercooling were always multigrained, as shown in Figure 20. Samples which were not undercooled also contained large shrinkage cavities connected to the surface. Notice also that most of the grains connect the surface of the drop to the shrinkage cavity. The tip of the drop shown in Figure 20B is the piece of unmelted Nb wire left in the sample to cause nucleation and prevent undercooling.

Using the equilibrium phase diagram [29] for the Nb-Ge system shown in Figure 21 and the measured temperature at the time of release, the undercooling for the Nb-Ge could be calculated once the cooling time until recalescence was measured by the infrared detectors. Undercooling data for the Nb-Ge alloys are presented in Table 3; all the drops were near 2.5 mm in diameter. The Nb-13 a/o Ge alloys are not included in Table 3 since

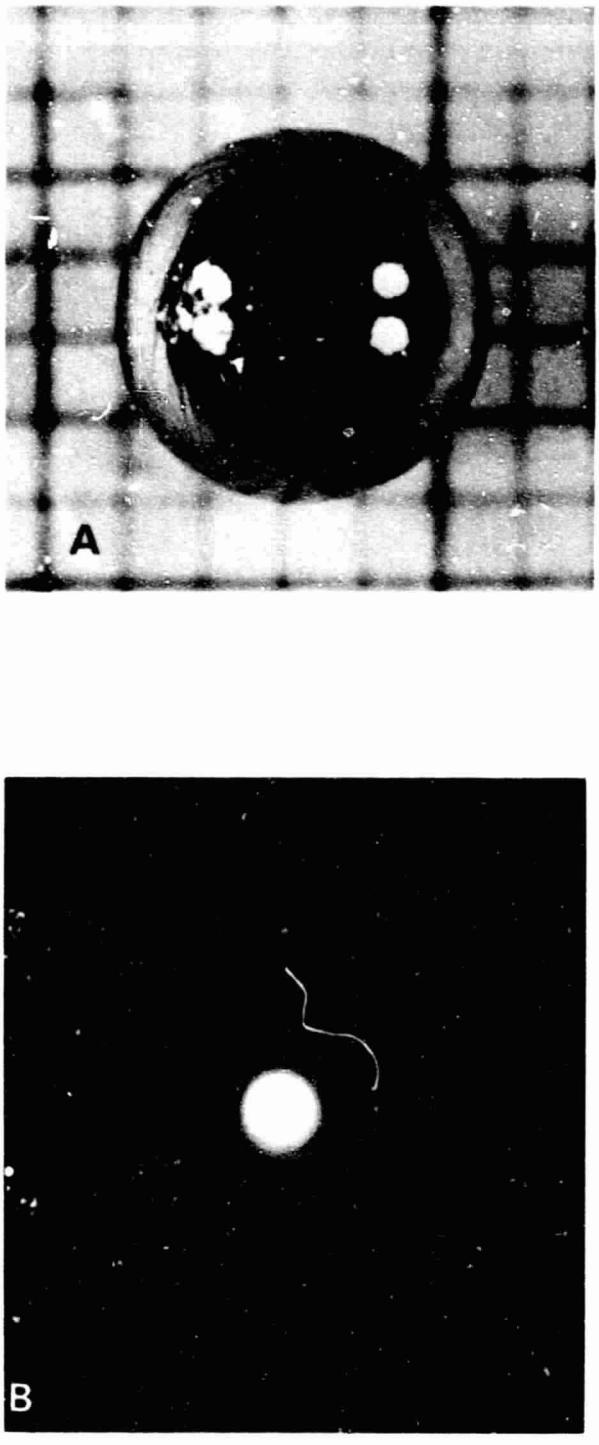


Figure 17. Typical Nb single crystal drop: (A) Photomicrograph at 8X; (B) Laue X-ray diffraction pattern for (110) direction.

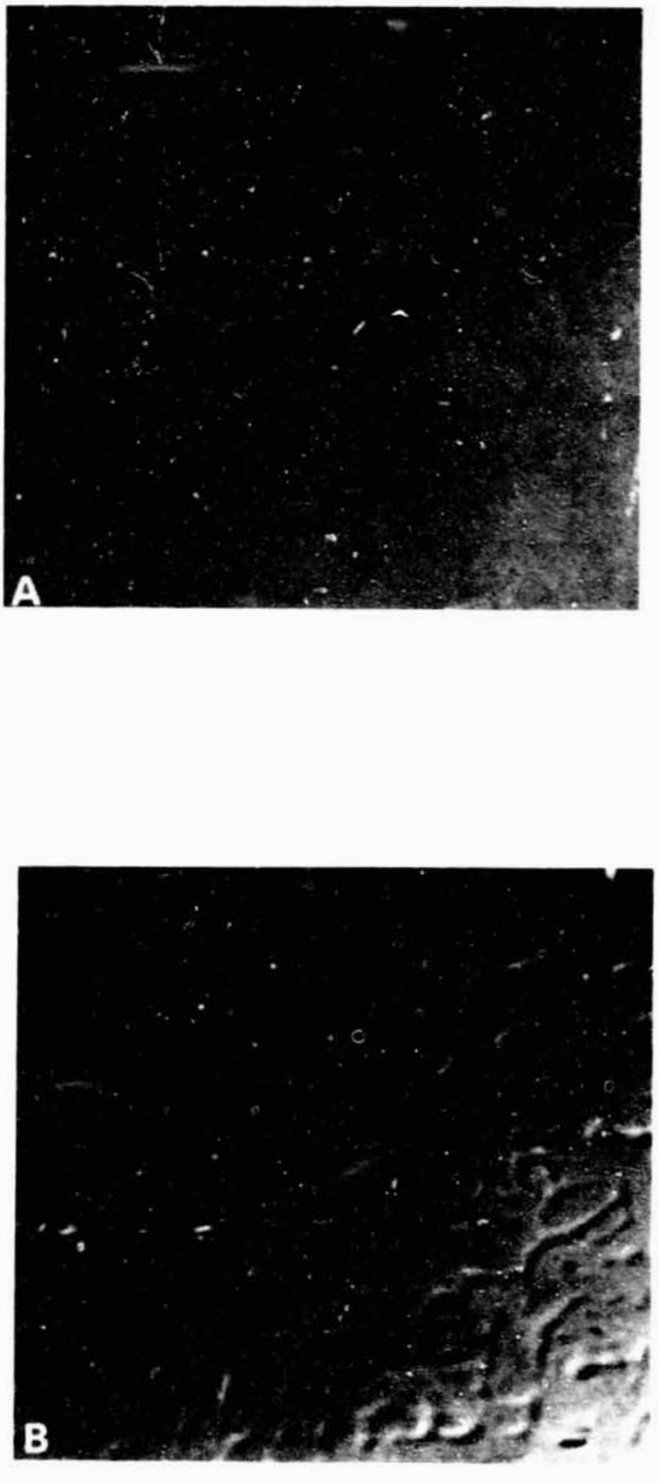


Figure 18. Scanning Electron Micrograph (SEM) of Nb drop surface (300X) with: (A) No undercooling; (B) Undercooling of 525 K.

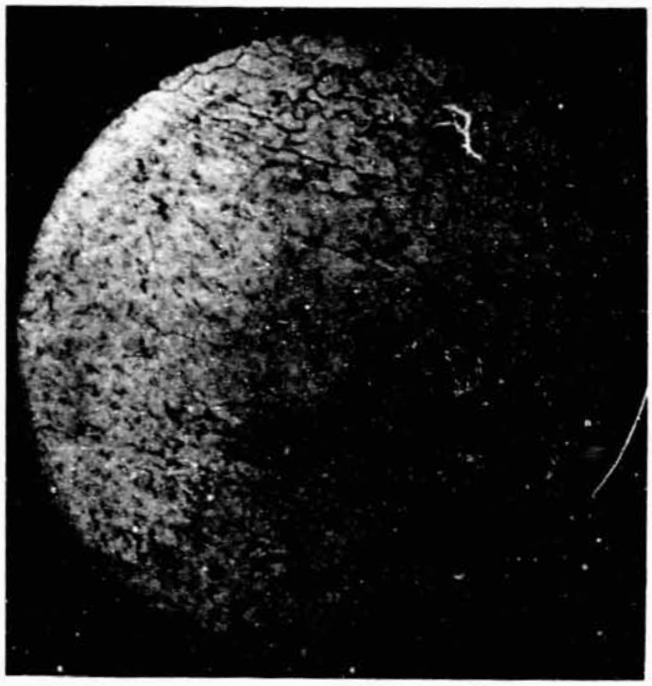

Figure 19. Cross-sectional photomicrograph (16X) of etched Nb drop Undercooled 525 K.

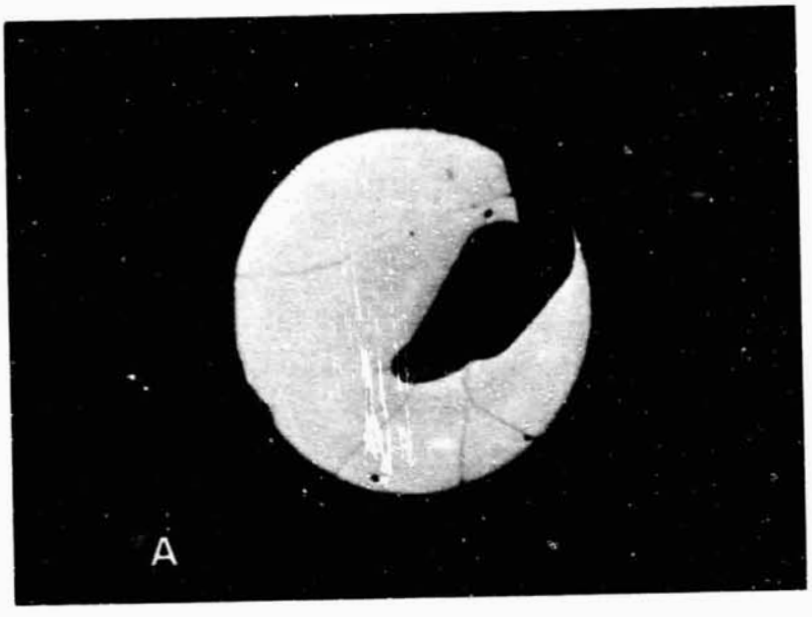


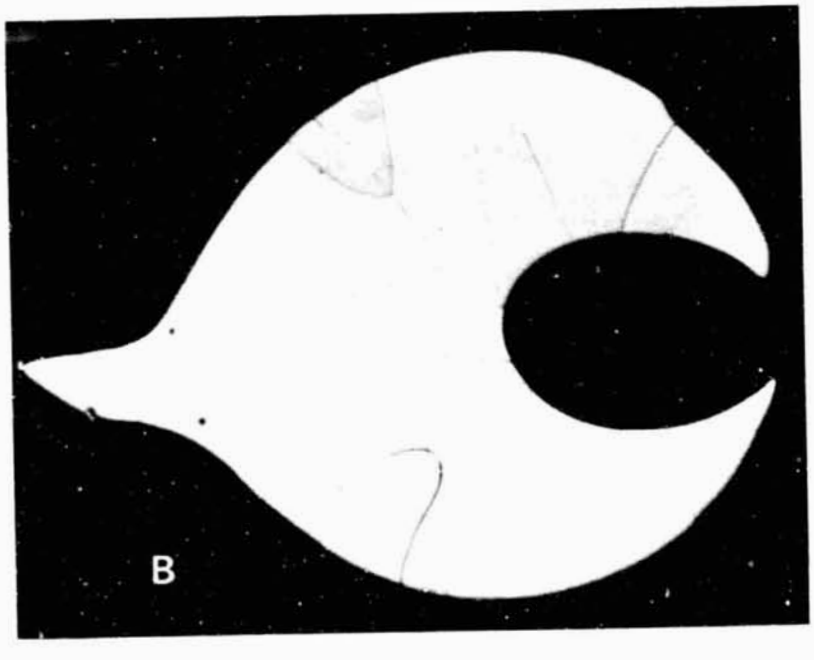


Figure 20. Cross-sectional photomicrograph of Nb samples with little or no undercooling.

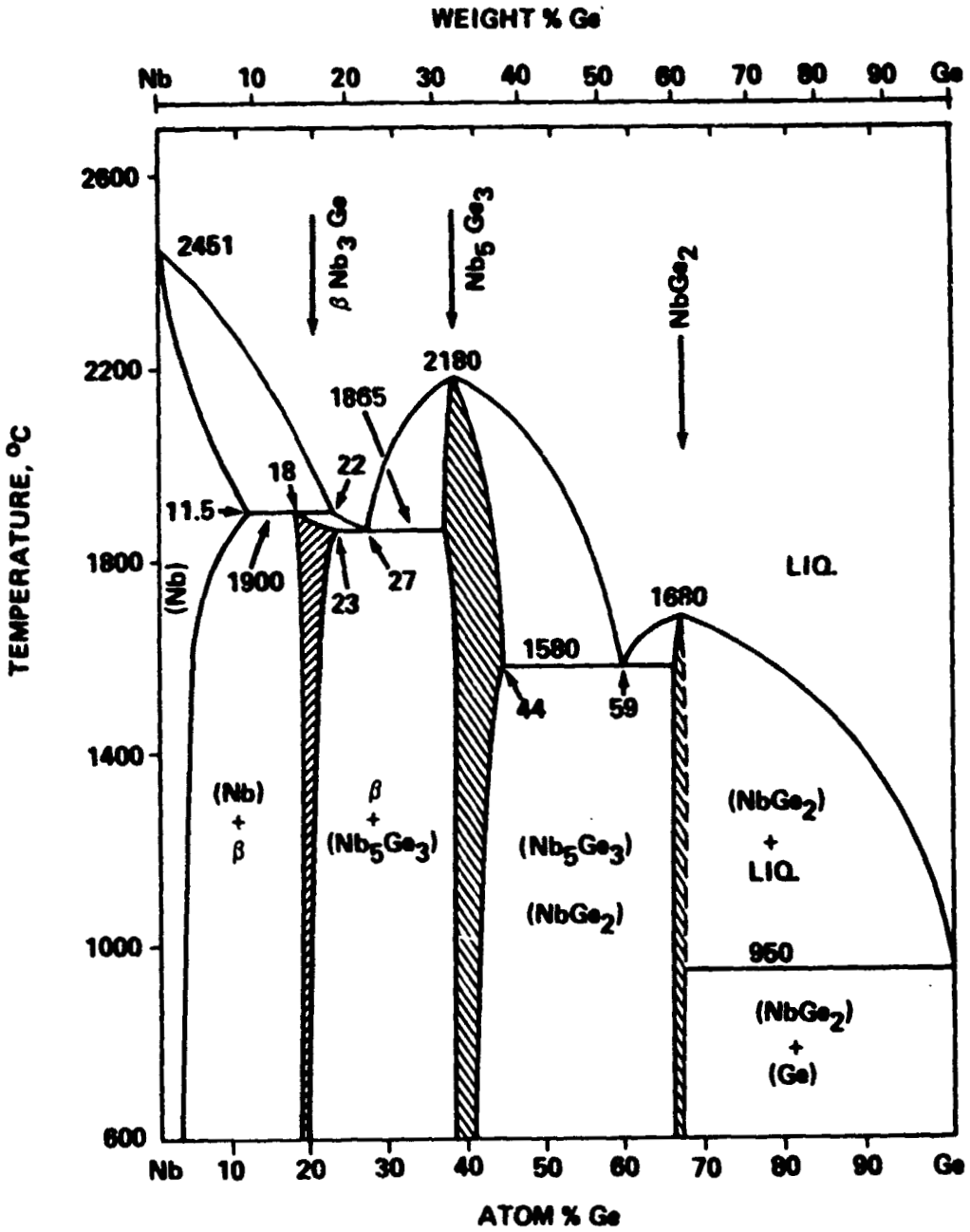


Figure 21. Phase diagram for Nb-Ge alloy system.

all efforts to detect undercooling for this composition have failed. If the 13 a/o Ge drops recalesced before coming into the field of view of the infrared detectors, the maximum amount of undercooling for these drops would be $< 200$ K. Undercoolings greater than 200 K would result in recalescence while in the field of view of the infrared detectors. Also, it was necessary to preheat the Nb-18 a/o Ge and Nb-22 a/o Ge alloy drops for approximately 3 min at about 1900 K to induce undercooling after the drop was released. Drops which were not preheated did not show evidence of undercooling.

From Table 3 it can be seen that the Nb-18 a/o Ge alloy drops consistently undercooled to approximately 20 percent of the liquidus temperature of 2337 K. Alloys of this composition usually were overheated approximatey 200 K above the liquidus temperature before release. The Nb-22 a/o Ge drops undercooled consistently to approximately 14 percent of the liquidus temperature of 2173 K, with overheatings in the range of 250 to 300 K. The corresponding undercoolings were as high as 500 K for the 18 a/o drops. The 22 a/o drops, although not as heavily undercooled as the 18 a/o Ge drops, were undercooled by as much as 300 K, which is certainly a significant amount of undercooling. It must be noted that the undercooling data presented in Table 3 do not necessarily represent the maximum amount of undercooling for these drops since all the alloy drops in this table, with the exception of DT 221, undercooled the full length of the drop tube and recalesced only upon impact with the quenching oil in the catcher. Consequently, it appears reasonable to expect significant improvements in undercooling Nb-Ge alloys in longer drop tubes. DT 221 recalesced slightly above the oil surface. The Nb-22 a/o Ge drops were overheated more than the 18 a/o drops and, together with the slower cooling rates due to lower processing temperatures, did not have as much time to undercool.

The amount of undercooling between the two compositions is evidenced by the shape of the retrieved particles. As shown in Figure 22, the 22 a/o Ge samples usually formed cup-shaped samples, while the 18 a/o Ge samples formed hemispherical drops. Since the 18 a/o Ge drops are more heavily undercooled, it would be expected that more of the sample would solidify upon recalescence, resulting in a less deformed drop. It is also possible that the 22 a/o Ge drops flowed into the cup shape before recalescence and were

TABLE 3

Nb-Ge ALLOY UNDERCOOLING

| Drop Number | % Ge | $T_i$ Release Temperature | $T_{ov}$ Amount of Overheating | $T_u$ Amount of Undercooling* | $\frac{T_u}{T_m}$ % |
|---|---|---|---|---|---|
| DT217 | 13 | 2597 | 80 | < 200 | < 8.0 |
| DT218 | 13 | 2607 | 90 | < 200 | < 8.0 |
| DT221 | 18 | 2457 | 120 | 495 | 21.2 |
| DT230 | 18 | 2520 | 183 | 477 | 20.4 |
| DT231 | 18 | 2570 | 233 | 457 | 19.6 |
| DT223 | 22 | 2473 | 300 | 290 | 13.3 |
| DT224 | 22 | 2434 | 261 | 299 | 13.7 |
| DT226 | 22 | 2408 | 235 | 305 | 14.0 |
| DT227 | 22 | 2431 | 258 | 302 | 13.9 |
| DT232 | 22 | 2468 | 295 | 295 | 13.6 |
| DT233 | 22 | 2429 | 256 | 299 | 13.7 |
| DT235 | 22 | 2405 | 233 | 307 | 14.1 |

*Note: The values of undercoolings for the 18 and 22 a/o Ge drops are not necessarily the maximum amount possible since these drops undercooled the complete length of the drop tube and recalesced only after impacting the quenching oil.

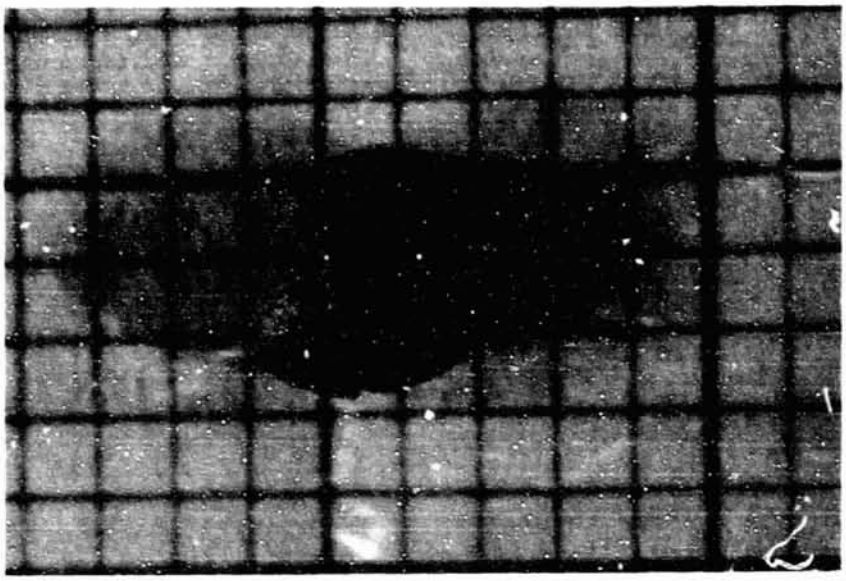

(B) Nb–18a/o Ge

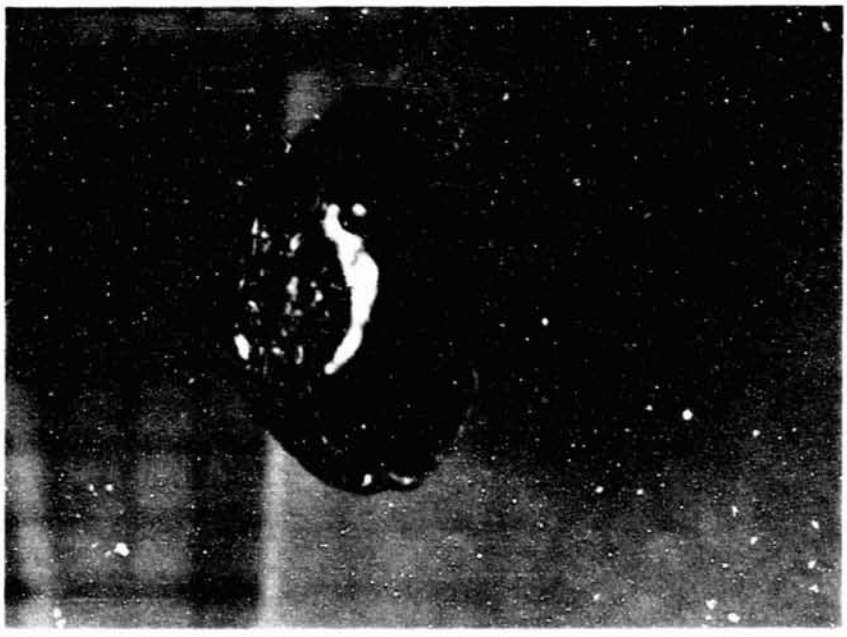

(A) Nb–22a/o Ge

Figure 22. Nb-Ge alloy samples undercooled in the drop tube.

therefore deformed as a liquid drop entering the quenching oil. The Nb-13 a/o Ge drops, which undercooled < 200 K, were spherical in shape with no deformation due to the oil.

The superconducting transition temperature of the samples appears to be favorably affected by undercooling. In Figure 23 the superconducting transitions of the undercooled samples can be compared to the transitions of the as-cast starting material. Notice that for both compositions the $T_c$ is increased significantly. It should also be noted that the transition of the Nb-22 a/o Ge drop is mostly above the transition temperature of pure Nb at 9.2 K. Since the only phase of the Nb-Ge system that has a $T_c$ above that of pure Nb is the metastable $\beta$ phase, it can be concluded that the Nb-22 a/o Ge drop samples contain the metastable $\beta$ phase. Therefore, the high $T_c$ metastable phase has been formed by rapid solidification after large amounts of undercooling. Additional work is necessary to further increase the $T_c$ of the $\beta$ phase contained in these samples.

It has, therefore, been shown that there exist significant differences between the undercooled and not undercooled samples for both the Nb and Nb-Ge alloy drops. Although these differences warrant in-depth analysis, it is not within the scope of this study to do so.

## VI. ESTIMATE OF ERRORS

By referring to equation (6), it can be concluded that the undercooling curves and therefore the undercooling temperatures are proportional to $\epsilon_T$, A, m, C, and the measured time of cooling before recalescence $t_c$. Also, from equation (5), it can be seen that the undercooling temperature will be proportional to the fourth power of the measured release temperature $T_i$. For pure Nb, $\epsilon_T$ is known to 3 percent and C is known to 2 percent. The mass is measured for all drops to an accuracy of 1 percent error, while the surface area is known to approximately 2 percent. The release temperatures are known very accurately ( < 0.5 percent error) due to the extensive calibration of the pyrometer. Also, the time of cooling before recalescence is measured to an accuracy of < 0.5 percent. Since the parameters involved in the calculation of the undercooling temperature $T_u$ are independent, the error in $T_u$ will be given by:

$$\frac{dT_u}{T_u} = \sqrt{\left(\frac{d\epsilon_T}{\epsilon_T}\right)^2 + \left(\frac{dA}{A}\right)^2 + \left(\frac{dm}{m}\right)^2 + \left(\frac{dC}{C}\right)^2 + \left(\frac{dt_c}{t_c}\right)^2 + \left(\frac{4dT_i}{T_i}\right)^2} \qquad (15)$$

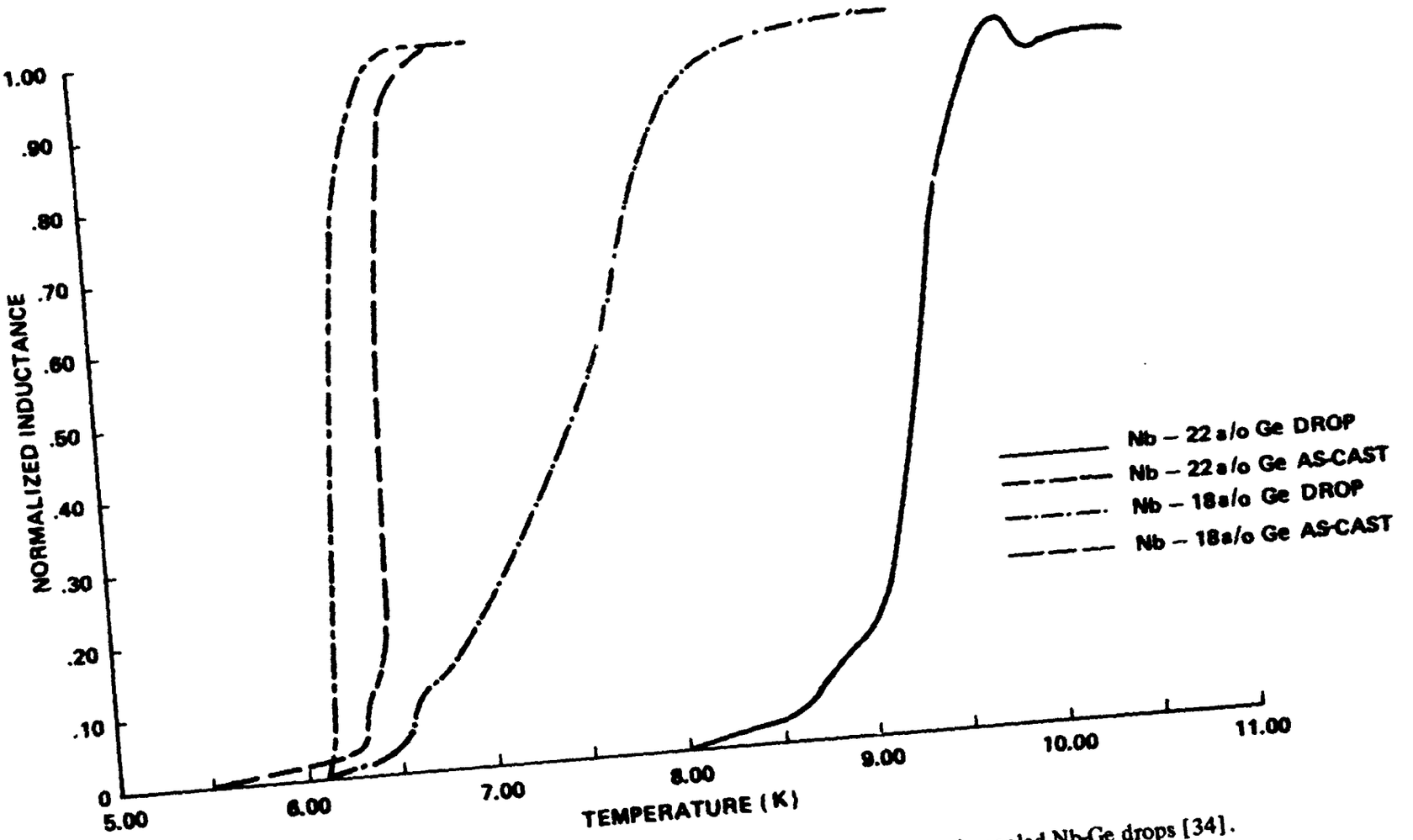


Figure 23. Comparison of transition temperatures of as-cast material and undercooled Nb-Ge drops [34].

which, by plugging in the discussed errors, results in an error of less than 5 percent for the calculated undercooling temperatures for Nb. Therefore, the undercooling temperatures for pure Nb should be accurate to less than 5 percent error or ± 25 K out of the reported 525 K undercooling for Nb.

To estimate the error for the undercoolings reported for the Nb-Ge alloy drops, an estimate of error for the measured emissivities and specific heats must first be made. From equation (11), it can be seen that error in the measured total emissivities will be proportioned to $\dot{Q}_l$, $\dot{Q}_w$, A, and $T^4$. Since the drop is still attached to the support wire during calorimetry studies, a 2.5 percent error in the surface area of the drop is expected. The value of the standard resistor is accurately known so that the 3 percent error in the heat input measurement is due to inaccuracies in the voltage measurement. The error due to the heat loss up the wire, $\dot{Q}_w$, should be less than 2 percent, while the temperature is again known to 0.5 percent.

Therefore, the error in the measured total emissivities should be less than 5 percent as given by:

$$\frac{d\epsilon_T}{\epsilon_T} = \sqrt{\left(\frac{dQ_l}{Q_l}\right)^2 + \left(\frac{dQ_w}{Q_w}\right)^2 + \left(\frac{dA}{A}\right)^2 + \left(\frac{4\,dT}{T}\right)^2} \quad . \tag{16}$$

The measured specific heats are dependent on $\epsilon_T$ as well as A, $T^4$, m, and $\dot{Q}_w$, as shown in equation (14). The error in the measured values of C will then be:

$$\frac{dC}{C} = \sqrt{\left(\frac{d\dot{Q}_w}{\dot{Q}_w}\right)^2 + \left(\frac{d\epsilon_T}{\epsilon_T}\right)^2 + \left(\frac{dA}{A}\right)^2 + \left(\frac{dm}{m}\right)^2 + \left(\frac{4dT}{T}\right)^2} \quad . \tag{17}$$

Equation (17) results in an error of 5 percent in the measured specific heats given in Table 1. By using the estimated errors of 5 percent for $\epsilon_T$ and 6 percent for C together with the errors in A, m, $t_c$, and $T_i$, as already discussed, the error in the measured undercooling temperatures for the Nb-Ge alloys will be approximately 8 percent as calculated from equation (15). This error amounts to ± 40 K for the 500 K undercoolings reported for Nb-18 a/o Ge and ±24 K for the 300 K undercoolings for Nb-22 a/o Ge. Thus the reported undercoolings in terms of percentage of the melting temperature are:

| | |
|---|---|
| Nb | $0.19\ T_m \pm 0.009\ T_m$ |
| Nb-18 a/o Ge | $0.20\ T_m \pm 0.016\ T_m$ |
| Nb-22 a/o Ge | $0.14\ T_m \pm 0.012\ T_m$ |

It should again be noted that these reported amounts of undercooling should not be considered as the maximum amounts possible for the Nb-Ge alloy drops since nucleation and recalescence occurred at the bottom of the drop tube.

## VII. CONCLUSION

The amount of undercooling of Nb and Nb-Ge alloy drops, while free falling in a 32 mm drop tube, has been measured. The technique used to measure the undercooling of the free-falling drops involves measuring to a high degree of accuracy ( $< 0.5$ percent) the length of time the sample undercooled before nucleation and recalescence occurred. Once the nucleation time was found, the amount of undercooling could be determined from the cooling curve calculated for each drop. The results show the Nb drops of up to 5 mm diameter were undercooled by 525 K, which relates to 19 percent of the melting temperature. This amount of undercooling is consistent with the empirical homogeneous nucleation limit suggested by Turnbull. However, the nucleation temperature of 2216 K also closely compares to the melting temperature of NbO at 2218 K. Thus, it may be possible that nucleation of the Nb drops may not have been homogeneous but instead heterogeneous, being induced by the formation of NbO on the surface of the falling molten Nb drops. It may, therefore, be possible to undercool Nb drops even more by prohibiting the formation of NbO on the surface. Further work is needed to confirm or disprove this postulate.

The technique was also demonstrated by measuring the amount of undercooling for Nb-Ge drops, which was $0.20\ T_m$ and $0.14\ T_m$ for the Nb-18 a/o Ge and Nb-22 a/o Ge alloy drops, respectively. The Nb-13 a/o Ge drops were undercooled by less than 200 K. Although the amount of undercooling for the Nb-18 a/o and Nb-22 a/o drops is significant, it does not necessarily represent the maximum amount possible since almost all of these alloy drops undercooled all the way down the drop tube and recalesced only after impacting the surface of the quenching oil.

To calculate the cooling rates for the Nb-Ge alloy drops, and therefore the amount of undercooling, it was first necessary to measure the total emissivities and specific heats using a high-temperature, containerless calorimeter. The calorimetry technique was first verified by measuring the values of $\epsilon_T$ and C for pure Nb. Since the measured and literature values for Nb agreed quite well, the properties were then measured for the Nb-Ge alloys. The results show that the measured values of $\epsilon_T$ for the Nb-Ge alloys were very close to $\epsilon_T$ for pure Nb. Also, the values of specific heats were found to be 356 J/kg for Nb-13 a/o Ge, 368 J/kg for Nb-18 a/o Ge, and 398 J/kg for Nb-22 a/o Ge. The liquid specific heats of the 18 and 22 a/o Ge alloys were also measured near the melting point; the result was 398 J/kg for both compositions, which matches closely the values of C in the solid state. Using these measured values, the cooling curves were then calculated for the Nb-Ge alloy drops.

Significant differences can be seen in the undercooled drops. The undercooled Nb drops exhibited single crystalline behavior with no visible major shrinkage cavity. The Nb drops with little or no undercooling consisted of many large grains and contained a large shrinkage cavity. Also, the undercooled Nb drops had a heavily dendritic surface structure, while the not undercooled drops were smooth. For the Nb-Ge drops, a significant increase in the superconducting transition temperature for the undercooled Nb-18 a/o Ge and Nb-22 a/o Ge alloy drops over the $T_c$ of the as-cast starting material was found. Since the $T_c$ of the Nb-22 a/o Ge drops was greater than the $T_c$ of Nb at 9.2 K, these drops must contain the metastable $\beta$ phase of $Nb_3Ge$. Additional work is proposed to further increase the $T_c$ of the $\beta$ phase present in the alloy drops.

The original use of this technique in the 32 m drop tube provides important undercooling information for processed materials so that a correlation between undercooling and resulting material properties may be made. A better understanding of solidification and material properties should result which may lead to the production of new and unique materials. The described techniques could also be used in any low-gravity, containerless processing environment.

## BIBLIOGRAPHY


1. D. Turnbull and R. E. Cech: J. Appl. Phys., Vol. 21 (1950).
2. J. H. Perepezko and D. H. Rasmussen: Met. Trans., Vol. 9A (1978) 1400.
3. B. Chalmers: Principles of Solidification (Wiley, New York, 1969) 114-124.
4. J. L. Walker, Jr.: Physical Chemistry of Process Metallurgy, Part 2, Ed. G. R. St. Pierre (Interscience, New York, 1961) 875.
5. T. Z. Kattamis and M. C. Flemings: Trans. AIME, 236 (1966) 1523.
6. T. Z. Kattamis and R. Mehrabian: J. Vac. Sci. Technology, Vol. 11, No. 6 (Nov./Dec. 1974) 1118.
7. J. H. Hollomon and D. Turnbull: J. of Metals, Trans. AIME (1951) 803-805.
8. J. P. Hirth: Met. Trans. A, Vol. 9A (1978) 401-404.
9. D. Turnbull: J. Chem. Phys., Vol. 20 (1952) 411.
10. S. Y. Shiraishi and R. C. Ward: Can. Met. Quar., Vol. 3 (1964) 197.
11. E. Meyer and L. Rinderer: J. Crystal Growth, Vol. 28 (1975) 197.
12. R. E. Cech and D. Turnbull: Trans. AIME, Vol. 206 (1956) 124.
13. L. L. Nelson: High Temp. Technology Proc. Int. Symp., Pacific Grove, California, 1967 (1969) 565.
14. L. L. Lacy, M. B. Robinson, and T. J. Rathz: J. Crystal Growth, Vol. 51 (1981) 47-60.
15. J. Steinberg, A. E. Lord, Jr., L. L. Lacy, and J. Johnson: Appl Phys. Lett., Vol. 38 (3) (1981) 135.
16. L. R. Testardi, J. H. Wernick, and W. A. Royer: Solid State Comm., Vol. 15 (1974) 1-4.
17. J. R. Gavaler: Appl Phys. Lett., Vol. 23, No. 8 (1973) 480-482.
18. E. M. Savitsky, E. Saur, C. J. Raub, and Y. V. Jefimov: Aeitschrift fuer Metallkinde, Vol. 68, No. 2 (1977) 123-134.
19. B. T. Matthias, T. H. Geballe, R. H. Willens, E. Corenzwit, and G. W. Hull, Jr.: Physical Review, Vol. 139, No. 5A (1965) A1501-A1503.
20. D. H. Shinger and R. Ozaki: Met. Trans., Vol. 6A (1975) 33.
21. L. L. Lacy, M. B. Robinson, T. J. Rathz, and D. B. Nisen: NASA Tech Brief, MFS 25242 (Spring 1980).

22. L. L. Lacy, M. B. Robinson, and D. B. Nisen: NASA Tech Brief, MFS 23923 (Spring 1979).

23. L. L. Lacy, M. B. Robinson, and D. B. Nisen: Containerless High Temperature Calorimeter Apparatus, U. S. Patent No. 4,248,083, Issued February 1979.

24. M. W. Zemansky: Heat and Thermodynamics (McGraw-Hill, New York, 5th ed., 1968).

25. Wollard and Rose, International Gravity Measurement (George Banta, Inc., 1963) 63.

26. A. J. Cezairliz an: J. Res. Natl. Bur. Std., Vol. 75A (1971) 565.

27. A. E. Sheindling, B. Ya. Berezin, and V. Ya. Checkhovskoi: High Temperature-High Pressure, Vol. 4 (1972) 611.

28. CRC Handbook of Chemistry and Physics, 56th ed. (Chemical Rubber Co., Cleveland, Ohio, 1976).

29. J. J. Jorda, R. Flu! ger, and J. Muller: J. Less Common Met., Vol. 62 (1978) 25.

30. D. W. Bonnel, J. A. Treverton, A. J. Valerga, and J. L. Margrave, Jr.: Temperature: Its Measurement and Control in Science and Industry, Vol. 4, Part 1, ed. H. H. Plumb (Inst. Soc. of America, 1972) 463.

31. D. W. Bonnel: Property Measurements and High Temperature Levitation Calorimetry Studies of Liquid Metals, PhD. Thesis, Rice University (1972).

32. M. B. Robinson: Radiative and Gas Cooling of Falling Molten Drops, NASA Report TM-78189 (1978).

33. R. P. Elliott: Constitution of Binary Alloys, 1st Suppl. (McGraw-Hill, New York, 1965) 262.

34. T. Rathz: Susceptibility Measurements on the Superconducting Properties of Nb-Ge Alloys, Master's Thesis, University of Alabama in Huntsville (1980).

35. H. J. Stoever: Applied Heat Transmission, (McGraw-Hill, New York, 1941) 35.

# APPENDICES

# APPENDIX A

## HEAT LOSS BY EVAPORATION

The amount of heat loss due to evaporation for a drop will be simply the product of the mass loss of the drop, $\Delta m$, and the heat of evaporation $H_V$ of the material lost. For the pure niobium drops, no measured mass loss occurred. For the niobium-germanium drops, a slight mass loss of less than 0.2 mg occurred. If it is assumed that all of the mass loss is due to Ge evaporating from the surface of the drop, then an estimate of this effect on the calculated cooling curves can be made. Using the heat of evaporation for Ge as 3.9 kJ/g [28], the total heat loss because of evaporation from a Nb-Ge drop will be 0.78 J. Since the drop time is only 2.6 s, most of the time that the drop is above 1700 K is during the heating and melting of the sample and not during the cooling time. If we, therefore, assume that not more than 25 percent of the mass loss occurs during actual cooling, then the heat loss while cooling 2.6 s will be 0.20 watts. By comparing this heat loss to that calculated from equation (2) (typical > 10 watts) it can be seen that evaporation heat loss will amount to less than 1 percent of the total heat loss. Therefore, evaporation heat loss effects were not included in the cooling curves calculated in the body of the text.

## APPENDIX B

### EFFECT OF REFLECTIONS ON HEAT LOSS BY RADIATION

Since a drop falling in the drop tube will have some light reflected back onto its surface, it was necessary to calculate the extent of this effect on the cooling rates of the drops. A worst case approximation of a drop in the drop tube can be made by assuming the drop is enclosed in a gray body sphere of radius $r_2$ and total emissivity $\epsilon_2$. The total heat loss by radiation from the drop of radius $r_1$ and total emissivity $\epsilon_T$ enclosed by this larger sphere will be given by [35]:

$$\dot{Q} = \sigma A \left[ \frac{1}{\frac{1}{\epsilon_T} + \left(\frac{r_1}{r_2}\right)^2 \left(\frac{1}{\epsilon_2} - 1\right)} \right] (T^4 - T_o^4) \quad , \tag{B-1}$$

where the outer sphere is considered to be at ambient temperature $T_o$. In equation (B-1), $\sigma$ is again the Boltzmann constant, T is the temperature of the drop, and A is the surface area of the drop. By choosing the radius of the outer sphere to be the radius of the drop tube ($\approx$ 5 cm) and the emissivity of the stainless steel drop tube to be 0.1, the heat loss of equation (B-1) can be calculated and compared to the heat of equation (2) in the text. This comparison has been made, with the result that the maximum error occurred for a large (5 mm diameter) sphere; it was less than 0.7 percent for all temperatures as compared to the heat loss calculated from equation (2). For smaller drops, this error would be less. Therefore, the reflections back onto the drop surface from the drop tube should have negligible effect on the cooling curves as calculated in the body of the text.

## APPENDIX C

### HEAT LOSS DUE TO THE SUPPORT WIRE

The heat loss from a droplet because of the support wire can be calculated by treating the wire as a series of small increments. The heat loss by radiation for the $n^{th}$ element of the wire will be:

$$\dot{Q}_{Rn} = \epsilon_w S_n T_n^4 \quad , \tag{C-1}$$

as taken from equation (2), with $\epsilon_w$ the total emissivity of the wire, $S_n$ the surface area of the $n^{th}$ increment of wire, and $T_n$ the temperature of the $n^{th}$ element. The effect of $T_o$ is negligible and has been omitted in equation (C-1). The heat loss due to conduction through the $n^{th}$ wire element will be:

$$\dot{Q}_{cn} = K A_n \left(\frac{dT}{dx}\right)_n \quad . \tag{C-2}$$

$A_n$ is the cross-sectional area of the wire, K is the thermal conductivity of the wire material, and $\left(\frac{dT}{dx}\right)_n$ is the thermal gradient across the $n^{th}$ wire element. Now consider the amount of heat being conducted into the $n^{th}$ element from the $(n-1)^{th}$ element and out of the $n^{th}$ element into the $(n+1)^{th}$ element. The difference will be:

$$\Delta\dot{Q}_{cn} = \dot{Q}_{c(n-1)} - \dot{Q}_{c(n+1)} = K A_n \left[\left(\frac{dT}{dx}\right)_{n-1} - \left(\frac{dT}{dx}\right)_{n+1}\right] \quad . \tag{C-3}$$

If we assume the heat profile along the whole length of the support wire is of the form:

$$T_n = T_s e^{-\beta X_n} \quad , \tag{C-4}$$

then

$$\left(\frac{dT}{dx}\right)_n = -T_s \beta e^{-\beta X_n} \quad , \tag{C-5}$$

where $T_s$ is the droplet temperature, $X_n$ is the distance from the droplet to the $n^{th}$ wire element, and $\beta$ is a constant to be determined. Plugging equation (C-5) into equation (C-3) gives:

$$\Delta \dot{Q}_{cn} = K A_n T_s \beta \left[ e^{-\beta X_{(n-1)}} - e^{-\beta X_{(n+1)}} \right] . \tag{C-6}$$

If we take the incremental elements of the support wire to be equal in length, then the distance to each $n^{th}$ element from the droplet will be:

$$X_n = n\alpha \quad , \tag{C-7}$$

where $\alpha$ is the length of each wire element. Plugging equation (C-7) into equation (C-6) gives:

$$\Delta \dot{Q}_{cn} = -K A_n T_s \beta \left[ e^{-\beta(n-1)\alpha} - e^{-\beta(n+1)\alpha} \right] , \tag{C-8}$$

which reduces to:

$$\Delta \dot{Q}_{cn} = +K A_n T_s \beta e^{-n\beta\alpha} \left[ e^{\beta\alpha} - e^{\beta\alpha} \right] \tag{C-9}$$

The difference in the heat flowing into the $n^{th}$ element and the heat flowing out of the $n^{th}$ element must be lost by radiation. Therefore, $\Delta \dot{Q}_{cn}$ must be equal to the heat lost by the $n^{th}$ element from radiation or:

$$\Delta \dot{Q}_{cn} = \epsilon_w S_n \sigma T_n^4 = \epsilon_w S_n \sigma T_s^4 e^{-4\beta\alpha n} \quad , \tag{C-10}$$

where equations (C-1) and (C-4) have been used. Equating equations (C-8) and (C-10) then gives:

$$-\epsilon_w S_n \alpha T_s^4 e^{-4\beta\alpha n} = -K A_n T_s \beta e^{-n\beta\alpha} \left[e^{\beta\alpha} - e^{-\beta\alpha}\right], \tag{C-11}$$

which reduces to:

$$\beta = \frac{2\epsilon_w \sigma \alpha T_s^3 e^{-3\beta\alpha n}}{K R_w \left[e^{\beta\alpha} - e^{-\beta\alpha}\right]} \tag{C-12}$$

by using

$$\frac{S_n}{A_n} = \frac{2\alpha}{R_w}, \tag{C-13}$$

where $R_w$ is the radius of the wire.

Now let $\alpha \to 0$ so that:

$$e^{\beta\alpha} - e^{-\beta\alpha} = 1 + \beta\alpha \ldots - 1 + \alpha\beta \ldots .$$

which goes to $2\alpha\beta$ for small $\alpha\beta$, which is the case for elements of support wire close to the droplet. Then:

$$\beta = \frac{\sigma \epsilon_w T_s^3}{K R_w \beta} e^{-3\beta\alpha n} \tag{C-14}$$

or

$$\beta^2 = \frac{\sigma \epsilon_w T_s^3 e^{-3\beta\alpha n}}{K R_w} \tag{C-15}$$

If we assume all the heat lost because of the wire leaves the droplet and enters the $0^{th}$ support wire element, then:

$$\beta_0^2 = \frac{\epsilon_w \sigma T_s^3}{K R_w} \tag{C-16}$$

The gradient across the $0^{th}$ element will then be:

$$\left.\frac{dT}{dx}\right|_{x=0} = -T_s \beta_0 = -\left(\frac{\epsilon_w \sigma T_s^5}{K R_w}\right)^{1/2} \tag{C-17}$$

by use of equations (C-5) and (C-15).

The heat conducted from the droplet into the $0^{th}$ element will then be, from equation (C-2),

$$Q_{co} = K A_o \left(\frac{dT}{dx}\right)_{x=0} = \pi \left[\epsilon_w \sigma T_s^5 K R_w^3\right]^{1/2} \tag{C-18}$$

by use of $A_o = \pi R_w^2$ and equation (C-16).

Thus equation (C-18) describes the heat loss from the droplet entering the wire which is the heat due to the wire of equation (9) in the text. It should be noted that several other models were tried and compared to the heat loss of equation (9). The results were that all the models compared to within 20 percent, which results in an inaccuracy of 2 percent in the total heat loss from the sphere since the heat loss because of the wire accounts for only 10 percent of the total heat loss.

## APPROVAL

## UNDERCOOLING MEASUREMENT IN A LOW-GRAVITY CONTAINERLESS ENVIRONMENT

By Michael B. Robinson

The information in this report has been reviewed for technical content. Review of any information concerning Department of Defense or nuclear energy activities or programs has been made by the MSFC Security Classification Officer. This report, in its entirety, has been determined to be unclassified.

ROBERT J. NAUMANN
Chief, Space Processing Division

CHARLES A. LUNDQUIST
Director, Space Sciences Laboratory



☆ U.S. GOVERNMENT PRINTING OFFICE 1981–740-066/448 REGION NO. 4